

1

Title

2

Neutrophilic inflammation promotes SARS-CoV-2 infectivity and augments the inflammatory responses in
airway epithelial cells

3

Author List

4

Calvert BA^{1,3}, Quiroz EJ^{1,2,3}, Lorenzana Z¹, Doan, N¹, Kim S⁴, Senger CN^{1,2}, Wallace WD⁵, Salomon MP⁶,
Henley J⁶, and Ryan AL^{1,2,3*#}

7

Author Affiliations

8

¹Hastings Center for Pulmonary Research, Division of Pulmonary, Critical Care and Sleep Medicine,
Department of Medicine, University of Southern California, Los Angeles, CA, USA

9

²Department of Stem Cell Biology and Regenerative Medicine, University of Southern California, Los
Angeles, CA, USA

10

³Department of Anatomy and Cell Biology, Carver College of Medicine, University of Iowa, Iowa City, IA,
USA

11

⁴The Salk Institute of Biological Studies, 10010 North Torrey Pines Road, La Jolla, CA, USA

12

⁵Department of Pathology, University of Southern California, Los Angeles, CA, USA

13

⁶Department of Medicine, University of Southern California, Los Angeles, CA, USA

14

ORCID IDs

15

0000-0003-1363-905X (A.L.R)

16

Contact Information

17

*Corresponding Author

18

Previously known as Amy L Firth

19

Amy L Ryan, PhD

20

Associate Professor: Anatomy and Cell Biology

21

Associate Director: Center for Gene Therapy

22

University of Iowa

23

1-400 Core, Basic Science Building (BSB)

24

51 Newton Road

25

Iowa City, IA 52242

29

E-mail: amy-l-ryan@uiowa.edu

30

Tel: 858 336 8667

31

32 **Abstract**

33 In response to viral infection, neutrophils release inflammatory mediators as part of the innate immune
34 response, contributing to pathogen clearance through virus internalization and killing. Pre-existing co-
35 morbidities correlating to incidence of severe COVID-19 are associated with chronic airway neutrophilia.
36 Furthermore, examination of COVID-19 explanted lung tissue revealed a series of epithelial pathologies
37 associated with the infiltration and activation of neutrophils, indicating neutrophil activity in response to SARS-
38 CoV-2 infection. To determine the impact of neutrophil-epithelial interactions on the infectivity and
39 inflammatory responses to SARS-CoV-2 infection, we developed a co-culture model of airway neutrophilia.
40 SARS-CoV-2 infection of the airway epithelium alone does not result in a notable pro-inflammatory response
41 from the epithelium. The addition of neutrophils induces the release of proinflammatory cytokines and
42 stimulates a significantly augmented pro-inflammatory response subsequent SARS-CoV-2 infection. The
43 resulting inflammatory response is polarized with differential release from the apical and basolateral side of
44 the epithelium. Additionally, the integrity of the epithelial barrier is impaired with notable epithelial damage
45 and infection of basal stem cells. This study reveals a key role for neutrophil-epithelial interactions in
46 determining inflammation and infectivity in response to SARS-CoV-2 infection.

47

48 **Keywords**

49 Airway Epithelium, Cell-Cell Interactions, Cytokines, Inflammation, Neutrophils, Viral Infection.

50

51 **Introduction**

52 Novel coronavirus infectious disease, COVID-19, is caused by the severe acute respiratory distress syndrome
53 related coronavirus 2, SARS-CoV-2 [1, 2]. While COVID-19 is associated with high hospitalization and
54 mortality rates, a substantial proportion of the population is asymptomatic or only experiences mild symptoms.
55 In response to viral infection neutrophils are the first and predominant immune cells recruited to the respiratory
56 tract [3]. Neutrophils release inflammatory mediators as part of the innate immune response and contribute
57 to pathogen clearance through virus internalization and killing [4]. While the protective versus pathological
58 role of neutrophils in the airways during viral response is poorly understood, it has been shown that the
59 number of neutrophils in the lower respiratory tract correlates to COVID-19 disease severity [5-7]. Infiltration
60 of neutrophils is also characteristic of other lung diseases associated with chronic infection and inflammation,
61 such as asthma, chronic obstructive pulmonary disease (COPD) and cystic fibrosis (CF). All these respiratory
62 diseases have been associated with an increased risk of developing severe COVID-19 [8]. Evaluating the
63 relationship between SARS-CoV-2 infection and pre-existing airway neutrophilia may provide critical insight
64 into how host and viral factors contribute to disease severity.

65 Neutrophils have an inherent capacity to recognize infectious agents, in addition to acting as sites of
66 infection and, in both cases, result in an acute inflammatory response [9]. Understanding the precise nature
67 of the inflammatory response and the pathophysiological consequences, could identify pathways for
68 therapeutic intervention based on early detection of a prognostic signature for COVID-19 outcomes. An
69 uncontrolled, hyper-inflammatory response, known as a “cytokine storm” can result from a massive influx of
70 innate leukocytes, inclusive of neutrophils and monocytes [10], and has been heavily implicated in patients
71 with severe COVID-19 [11, 12]. Cytokine storm and presence of pro-inflammatory mediators can be a
72 predictor of disease severity and often leads to acute respiratory distress syndrome (ARDS), and eventually
73 respiratory failure [13]. Retrospective studies have also demonstrated that elevated levels of interleukin-6 (IL-
74 6) are a strong predictor of mortality over resolution [14], and tumor necrosis factor alpha (TNF α) is increased
75 in severe compared to moderate cases [15].

76 Despite their importance in anti-viral immunity and response to viral pathogens, neutrophils have been
77 somewhat overlooked for their role in the pathogenesis of SARS-CoV-2 infection [16-18]. It has been shown
78 that the number of neutrophils in the lower respiratory tract correlates to disease severity in other viral

79 infections, including influenza A infection [19] and, more recently, to also be a feature of COVID-19 pathology
80 [18]. Several studies have highlighted the importance of neutrophils in the response to SARS-CoV-2 infection
81 [17, 18, 20, 21] and clinically neutrophil-lymphocyte ratios (NLR) are becoming an important hallmark of
82 severe COVID-19 [22]. Furthermore, the expression of angiotensin converting enzyme 2 (ACE2) on
83 neutrophils has also been demonstrated [23-26]. These studies, however, have primarily focused on the
84 recruitment of neutrophils post-infection and the production of neutrophil extracellular traps and lack insights
85 into the infection of airways with pre-existing neutrophilia and other neutrophil functional responses such as
86 inflammatory cytokine production and viral internalization.

87 In this study, the relationship between SARS-CoV-2 infection and pre-existing airway neutrophilia in
88 differentiated airway epithelium was evaluated through the adaption of a co-culture infection model previously
89 used to study viral infections *in vitro* [27]. Primary neutrophils were isolated from peripheral blood and co-
90 cultured with differentiated primary tracheo-bronchial airway epithelium prior to infection with live SARS-CoV-
91 2 virus for 4 hours to characterize the earliest stages of infection. Changes in the inflammatory profile and
92 epithelial response were comprehensively evaluated to determine the impact of pre-existing neutrophilia on
93 SARS-CoV-2 infection of the airway epithelium.

94

95 **Materials and Methods**

96 **Isolation of neutrophils from peripheral blood**

97 Neutrophils were isolated from fresh human peripheral blood with patient consent and approval of the
98 Institutional Review Board (IRB) of the University of Southern California (USC), protocol #HS-20-00546.
99 CD15-expressing neutrophils were isolated using the EasySep™ direct neutrophil isolation kit (Stem Cell
100 Technologies, Seattle, WA) within 1 hour of the blood draw as per the manufacturer's instructions. Briefly, 5
101 ml of peripheral blood was collected into 10 ml EDTA vacutainers (Becton Dickinson, Franklin Lakes, NJ).
102 From this, 3 ml was diluted 1:1 with PBS (Thermo Fisher Scientific, Waltham, MA) and kept on ice for purity
103 analysis by flow cytometry. The remaining 2 ml was transferred to a 5 ml polystyrene round bottomed tube
104 (Genesee Scientific, San Diego, CA) and gently combined with 100 µl of isolation cocktail and 100 µl of
105 RapidSpheres™ (Stem Cell Technologies). After incubation at room temperature for 5 mins, 1.8 ml of 1 mM
106 EDTA was added, gently mixed, and placed into the EasySep™ Magnet (Stem Cell Technologies) for 5 mins.
107 The enriched cell suspension was placed into the EasySep™ Magnet for an additional 5 mins and decanted
108 into a fresh tube. Approximately 4.25×10^6 cells were isolated from 5 ml of peripheral blood.

109 **Flow activated cell sorting (FACS)**

110 To validate the purity of neutrophils isolated from peripheral blood; 1×10^7 CD15⁺ freshly isolated human
111 neutrophils were resuspended in 100 µl FACS buffer (PBS, 0.5mM EDTA, 1% FBS, 0.1% BSA) and fresh
112 whole human blood diluted 1:5 in FACS buffer and supplemented with 5 µl of human TruStain Fc receptor
113 blocker (Biolegend, San Diego, CA) for 5 mins on ice. Cells were then incubated with anti-human CD15 PE
114 (Biolegend) for 1 hour prior to FACS analysis. Cells were analyzed on the SORP FACS Symphony cell sorter
115 (BD Biosciences) in the Flow Cytometry Facility at USC using FACS Diva software and all analyses was
116 carried out in Flow Jo V10.8.0 (BD Biosciences).

117 **Air-liquid interface (ALI) differentiation of airway epithelium**

118 Primary human airway basal epithelial cells (HBECs) were isolated from explant human lung tissue as
119 previously described [28] and with approval of IRB at USC (protocol #HS-18-00273). For this study, HBEC
120 donors were randomly paired with blood neutrophil donors (detailed in **supplemental table S2&3**). HBECs
121 were expanded for 1 to 4 passages in airway epithelial cell growth media (AEGM, Promocell, Heidelberg, DE)

122 and transitioned to Pneumacult Ex+ (Stem Cell Technologies) for 1 passage, prior to growth on Transwells.
123 Cells were routinely passaged at 80% confluence using AccutaseTM (Stem Cell Technologies) and seeded at
124 5 x 10⁴ cells per 6.5 mm polyethylene (PET) insert with 0.4 µm pores (Corning, Corning, NY). Media was
125 changed every 24-48 hours and transepithelial electrical resistance (TEER) was monitored every 24-48 hours
126 using an EVOM3 epithelial volt-ohm meter (World Precision Instruments, Sarasota, FL). At resistances ≥
127 450Ω ^cm², cells were air lifted by removing the apical media and washing the apical surface with phosphate
128 buffered saine (PBS, Sigma-Aldrich, St Louis, MO). The basolateral media was replaced with Pneumacult
129 ALI media (Stem Cell Technologies) and changed every 2 to 3 days for up to 40 days.

130 **SARS-CoV-2 culture**

131 Vero E6 cells overexpressing ACE2 (VeroE6-hACE2) were obtained from Dr. Jae Jung and maintained in
132 DMEM high glucose (Thermo Fisher Scientific, Waltham, MA), supplemented with 10% FBS (Thermo Fisher
133 Scientific, Waltham, MA), 2.5 µg/ml puromycin (Thermo Fisher Scientific, Waltham, MA) at 37°C, 5% CO₂ in
134 a humidified atmosphere in the Hastings Foundation and The Wright Foundation Laboratories BSL3 facility
135 at USC. SARS-CoV-2 virus (BEI resources, Manassas, VA) was cultured and passaged 4 times in VeroE6-
136 hACE2 cells and harvested every 48 hours post-inoculation. Plaque forming units (PFU) were determined
137 using a plaque assay by infecting a monolayer of VeroE6-hACE2 cells with serial dilutions of virus stocks and
138 layering semi-solid agar. Plaques were counted at day 3 post infection to determine PFU. Virus stocks were
139 stored at -80°C.

140 **SARS-CoV-2 infection**

141 Differentiated airway epithelium at ALI was cultured with addition of 50 µl of PBS to the apical surface and
142 incubated at 37°C, 5% CO₂ in a humidified atmosphere. After 10 minutes PBS was removed to eliminate the
143 mucus build-up on the apical surface. The basolateral culture media was removed and replaced with 400 µl
144 of assay media (Bronchial Epithelial Growth Media (BEGM), Lonza, Walkersville, MA), without the addition of
145 bovine pituitary extract, hydrocortisone & GA-1000, for 1 hour prior to the addition of neutrophils. Freshly
146 isolated neutrophils were diluted to 5 x10⁶ cells/ml in Hank's Balanced Salt Solution (with Mg²⁺ and Ca²⁺)
147 (Thermo Fisher Scientific, Waltham, MA) and 20 µl of this suspension was seeded onto the apical surface of
148 the ALI cultures. Monocultures of airway epithelium and neutrophils were used as controls. The neutrophil-

149 epithelial co-cultures were incubated for 1 hour during which they were transferred to the BSL3 facility for
150 infection. Co-cultures were infected with 1×10^4 PFU of SARS-CoV-2 in 100 μ l of OptiMEM (Thermo Fisher
151 Scientific, Waltham, MA) added to the apical surface. Infected cell cultures were incubated for 4 hours at
152 37°C, 5% CO₂ in a humidified atmosphere. After infection, the apical and basolateral supernatants were
153 collected, and SARS-CoV-2 was inactivated with 1% Triton-X (Sigma-Aldrich, Burlington, MA) in PBS for 1
154 hour. Culture supernatants were stored at -20°C until required.

155 **Validation of virus inactivation**

156 SARS-CoV-2 virus was inactivated by addition of 10% Triton-X to supernatants to generate a final
157 concentration of Triton-X of 1% and incubating at room temperature for 1 hour. PFU was quantified using a
158 plaque forming assay with ACE2 over-expressing Vero E6 cells (VeroE6-hACE2). Serial dilutions of SARS-
159 CoV-2 virus were performed from a stock concentration of 1×10^5 PFU/ml and inactivated with 1% Triton-X at
160 room temperature for 1 hour and used to infect Vero E6 cells for a total of 4 days. Cells were monitored
161 routinely for cytopathic effects using the Revolve microscope (Echo Laboratories, San Diego, CA).

162 **RNA isolation and qRT-PCR**

163 RNA was collected in 100 μ l of Trizol (Thermo Fisher Scientific, Waltham, MA) per insert and incubated for
164 15 mins at room temperature. Cell isolates were gently mixed by pipetting up and down. An additional 900 μ l
165 of Trizol was added and cell isolates were collected and stored at -80°C until required. Cellular RNA was
166 isolated by either phenol/chloroform extraction or using the Direct-zol RNA Microprep kit (Zymo Research,
167 Irvine, CA). RT-qPCR was performed in 384 well plates on an Applied Biosystems 7900HT Fast Real-Time
168 PCR system using the QuantiTect Virus Kit (Qiagen, Redwood City, CA) and SARS-CoV-CDC RUO primers
169 and probes (Integrated DNA Technologies (IDT), Coralville, IA). Briefly, each 5 μ l reaction contained 1 μ l 5x
170 QuantiTect Virus Master Mix, 500 nM forward primer, 500 nM Reverse Primer, 125 nM Probe, 10 ng DNA,
171 0.05 μ l QuantiTect Virus RT Mix, and DNase/RNase-free water up to a final volume of 5 μ l. Calibration curves
172 for RNaseP primers/probe was performed with 10-fold dilutions of RNA from uninfected Calu3 cells (ATCC,
173 Manassas, VA) from 100 ng to 0.01 ng per reaction. Calibration curves for N1 primers were performed on 5
174 ng of RNA from uninfected Calu3 cells per reaction spiked with 10-fold dilutions from 50 ng to 0.005 ng of

175 RNA from Calu3 cells collected 48 hours post infection. Relative gene expression was calculated using the
176 Pfaffl method [29].

177 **Immunohisto-/cyto-chemistry**

178 Primary human lung tissue from post-mortem or surgical resection donors (detailed in **supplemental table**
179 **S1**) was fixed in 10% neutral buffered Formalin (Thermo Fisher Scientific, Waltham, MA). The tissue was then
180 dehydrated in 70% ethanol (Thermo Fisher Scientific, Waltham, MA) prior to embedding in paraffin blocks for
181 sectioning. Tissue sections were mounted on positively charged slides (VWR, Visalia, CA) and tissue was
182 rehydrated through sequentially decreasing concentrations of ethanol (100% - 70%) and finally water. Slides
183 were stained sequentially with Hematoxylin and then Eosin and imaged on the Olympus microscope IX83
184 (Olympus, Waltham, MA). Alternatively, tissue slides were incubated overnight at 60°C in Tris-based antigen
185 unmasking solution (Vector Laboratories, Burlingame, CA) before permeabilization in 3% BSA, 0.3% Triton-
186 X 100 in PBS for 1 hour and blocking in 5% normal donkey serum (Jackson ImmunoResearch, West Grove,
187 PA) for 1 hour at room temperature. *In vitro* co-cultures were fixed in 4% PFA (Thermo Fisher Scientific,
188 Waltham, MA) for 1 hour at room temperature and stored in PBS at 4°C to be used for
189 immunohisto/cytochemistry. Co-cultures were then permeabilized and blocked in 3% BSA, 0.3% Triton-X 100
190 in PBS for 1 hour and blocking in 5% normal donkey serum (Jackson ImmunoResearch, #017-000-121) for
191 1 hour at room temperature. Tissue sections and *in vitro* cultures were subsequently stained with the
192 antibodies or RNAScope probes listed in **supplemental table S4**. Slides were mounted in Fluoromount-G
193 (Thermo Fisher Scientific, Waltham, MA) and imaged on a DMi8 fluorescent microscope (Leica, Buffalo
194 Grove, IL) or a Zeiss LSM 800 confocal microscope (Zeiss, Dublin, CA).

195 **Transepithelial Electrical Resistance**

196 Pre-warmed assay media (200 µl) was added to the apical surface of the cultures and TEER was measured
197 using an EVOM-3 meter (World Precision Instruments).

198 **Meso Scale Discovery cytokine assay**

199 50 µl of apical and 50 µl basolateral cell culture supernatants were analyzed for cytokines using the Meso
200 Scale Discovery (MSD) V-plex Viral Panel 1 Human Kit (Meso Scale Diagnostics, Rockville, MA) as per the
201 manufacturer's instructions. Briefly, 1:5 dilutions of cell supernatant samples were diluted in PBS containing

202 1% Triton-X. Samples were added to the MSD plate along with a 7-point 4-fold serial dilution (concentrations
203 related to certificate of analysis for each individual standard) of protein standards diluted in PBS with 1%
204 Triton-X. The MSD plate was sealed, and samples incubated at room temperature for 2 hours on a plate
205 shaker (ThermoFisher Scientific, Waltham, MA) at 700RPM. The plate was washed 3x in wash buffer and 25
206 μ l of secondary antibody was added to each well. Plates were sealed and incubated at room temperature on
207 a plate shaker at 700RPM for a further 2 hours in the dark. Plates were washed 3x with wash buffer and 50
208 μ l of 2x read buffer (MSD R92TC) was added to each well. The plates were read on the MESO Sector S 600
209 (Meso Scale Diagnostics) and concentrations determined against the standard curves.

210 **Meso Scale Discovery SARS-CoV-2 Spike protein assay**

211 25 μ l of apical and 25 μ l basolateral cell culture supernatants were analyzed for cytokines using the MSD S-
212 plex SARS-CoV-2 Spike Kit as per the manufacturer's instructions. Briefly, plates were washed 3x in wash
213 buffer (PBS 0.05% Tween-20) and coated with 50 μ l of coating solution (1:40 dilution of Biotin SARS-CoV-2
214 spike antibody; 1:200 dilution of S-PLEX Coating reagent C1 in Diluent 100) and incubated at room
215 temperature on a plate shaker at 700RPM for 1 hour. Plates were then washed 3x in wash buffer and blocked
216 in 25 μ l blocking solution (1:100 dilution of Blocker s1 in Diluent 61) per well. Samples were added to the
217 MSD plate along with a 7-point 4-fold serial dilution (concentrations related to certificate of analysis for each
218 individual standard) of protein standards diluted in PBS with 1% Triton-X. Plates were incubated at room
219 temperature on a plate shaker at 700RPM for 1.5 hours. Plates were washed 3x in wash buffer and 50 μ l per
220 well of TURBO-BOOST antibody (1:200 dilution of TURBO-BOOST SARS-CoV-2 Spike antibody in Diluent
221 59) was added to each well and plates were incubated at room temperature on a plate shaker at 700RPM for
222 1 hour. Plates were washed 3x in wash buffer and 50 μ l per well of Enhance Solution (1:4 dilution of S-plex
223 Enhance E1 1:4 dilution of S-plex Enhance E2 and 1:200 dilution of S-plex Enhance E3 in molecular biology
224 grade water) was added. Plates were incubated at room temperature on a plate shaker at 700RPM for 30
225 mins. Plates were washed 3x in wash buffer and 50 μ l of Detection solution (1:4 dilution of S-plex Detect D1
226 and 1:200 dilution of S-plex detect D2 in molecular biology grade water) was added to each well. Plates were
227 incubated at 27°C on a plate shaker at 700RPM for 1 hour. Plates were washed 3x in wash buffer and 150 μ l
228 on MSD GOLD Read Buffer B was added to each well. Plates were read immediately on a MSD 1300 MESO

229 QuickPlex SQ 120 plate reader (Meso Scale Diagnostics) and concentrations determined against the
230 standard curve.

231 **Viral Internalization Assay**

232 CD15+ neutrophils were seeded at 20,000 cells per well in in HBSS with or without 15 μ M Cytochalasin D
233 (Sigma Aldrich, Burlington) black walled 96 well plates (Thermo Fisher Scientific, Waltham, MA) for 1 hour to
234 allow for attachment. Cells were then infected with SARS-CoV-2 at 2 MOI (80 μ l at 5×10^5 PFU/ml) for 4
235 hours. Cells were then washed 2 x with PBS and fixed in 4% PFA. Cells were stained for SARS-CoV-2 RNA
236 via RNAScope and DAPI as per the manufacturer's instructions. Whole wells were supplemented with 50 μ l
237 of PBS post staining and well were scanned on the DMi8 fluorescent microscope (Leica, Buffalo Grove, IL)).
238 Total cell number was determined by total frequency of DAPI particles and infected cells determined by SARS-
239 CoV-2 particle signal in proximity to DAPI. Images were analyzed with ImageJ software 1.52n (National
240 Institute of Health, Bethesda, MA).

241 **Data Analysis and Statistics**

242 All data are presented as mean \pm S.E.M. Statistical analysis is dependent upon the data set and is specifically
243 indicated in each figure. For comparisons of 2 groups. a two-tailed unpaired Student's T-test was used. For
244 more than 2 groups, an analysis of variance (ANOVA) was used with a post hoc Tukey test. Significance is
245 determined to be $P < 0.05$. All data represents a minimum of three independent biological replicates ($N=3$),
246 each with 3 experimental replicates ($n=3$). Data was presented and analyzed using Graph Pad prism v8.4.3
247 (GraphPad, San Diego, CA).

248

249 **Results**

250 **In vitro models of neutrophilic airways have significant, polarized inflammatory responses to SARS-
251 CoV-2 infection.**

252 Given the prevalence of neutrophilia in the airways of patients with chronic airway disease [30] and its
253 association with other SARS-CoV-2 co-morbidities, such as diabetes mellitus [31] and hypertension [32, 33],
254 the impact of chronic neutrophilic airway inflammation in the initial stages of SARS-CoV-2 infection was
255 evaluated. We adapted a neutrophilic airway *in vitro* model, previously described by Deng and colleagues
256 [27], co-culturing CD15⁺ peripheral blood polymorphonuclear leukocytes (PMNs) with primary HBECs
257 differentiated at the ALI and infected these cultures with live SARS-CoV-2 virus for 4 hours, shown in the
258 schematic in **figure 1a**. This 4-hour time point allows for profiling of the initial stages of infection and acute
259 phase cellular viral response, i.e., neutrophil degranulation. The short time frame for analysis was chosen to
260 eliminate significant viral replication and thus anticipate any detectable intracellular viral load is as a result of
261 initial infection [34], and to allow for optimal investigation into neutrophil function without loss of viability
262 interfering with the assays due to the relatively short half-life of neutrophils. Prior to infection we confirmed
263 the expression of ACE2 and Transmembrane Serine Protease 2 (TMPRSS2) in our *in vitro* airway epithelium
264 models (**supplementary figure S1**). While ACE2 RNA was relatively low in expression across basal,
265 secretory and multiciliated cells (**supplementary figure S1a-c**) at the protein level a predominant
266 colocalization was detected with multiciliated cells in the airways (**supplementary figure S1a, d-f**). This data
267 supported by similar analysis of human lung tissues (**supplementary information and supplementary
268 figure S2**) where we observed a similarly low level of expression in RNA in basal, secretory and multiciliated
269 cells (**supplementary figure S2a-b**) while protein, detected by IF, was associated with multiciliated cells and
270 cells in submucosal glands (**supplementary figure S2c-f**). Confirmation of ACE2 expression at the RNA and
271 protein level in human lung tissues and our *in vitro* model supports currently published data evaluating ACE2
272 in human lung tissue [35-37].

273 In our model system the apical side of the epithelium comprises predominantly multiciliated and secretory
274 cells directly exposed to neutrophils and the virus, the basolateral side predominantly comprises of basal
275 cells. To understand the immediate inflammatory response of the airway epithelium to SARS-CoV-2 infection
276 we evaluated both the apical and basolateral cell culture supernatants using the meso scale discovery (MSD)

277 cytokine assay. All experiments were carried out using three independent HBEC donors and three
278 independent neutrophil donors ensuring significant biological variability in our model system. As shown in
279 **figure 1b&c** a differential inflammatory profile exists between the apical and basolateral compartments.
280 Focusing first on the apical cytokine and chemokine release, in the absence of neutrophils, there were,
281 surprisingly. no significant changes in cytokine release from the airway epithelial cells upon SARS-CoV-2
282 infection (**figure 1b**). The addition of neutrophils to the model, creating a neutrophil-epithelial co-culture in the
283 absence of any infection, resulted in a significant secretion of interferon gamma (IFNy, $634\pm1.6\%$, $p<0.01$)
284 and IL-10 ($273\pm11.6\%$, $p<0.01$) at the apical surface with notable, but not statistically significant, increases in
285 tumor necrosis factor alpha (TNF α) (**figure 1b**). Like the apical release, in the airway only cultures only
286 basolateral release of interleukin-8 (IL-8), which increased from 6180 ± 1751 to 52996 ± 17121 pg/ml, $p<0.001$,
287 and basolateral release of IL-10, which increased from 74.42 ± 15.36 to 142.4 ± 12.82 pg/ml ($p<0.05$), were
288 significantly changed in response to SARS-CoV-2 infection (**figure 1c**). As IL-8 is a major chemoattractant
289 for neutrophils this suggests that the basolateral surface responds to viral infection by releasing IL-8 to recruit
290 neutrophils to infection site [38-40]. The addition of neutrophils to the airway stimulated the release of IFNy
291 ($321\pm4.1\%$, $p<0.05$) and IL-10 ($341\pm8.5\%$, $p<0.01$) and additionally significantly increased the release of IL1-
292 β ($557\pm4\%$, $p<0.0001$), IL-4 ($220\pm3\%$, $p<0.0001$), IL-6 (761.9 ± 120.7 , $p<0.05$) and TNF α (274 ± 57.8 , $p<0.01$)
293 from the basolateral surface (**figure 1c**). Interestingly, the presence of neutrophils did not stimulate significant
294 changes in IL-8 secretion from the basolateral surface supporting the role for IL-8 in the recruitment phase of
295 airway neutrophilia, already established in our neutrophilic airway model (**figure 1c**) [41, 42]. This data
296 demonstrates that a pro-inflammatory niche is driven primarily by the neutrophils, likely through degranulation.
297 Based on this information we added neutrophils to our airway epithelium to create a pro-inflammatory niche
298 recreating aspects of chronic airway inflammation in the human lung in an *in vitro* model.
299 Infection of the neutrophilic airway models with live SARS-CoV-2 virus was compared directly to both the
300 infection in the absence of neutrophils and the neutrophilic airway in the absence of infection. Changes in
301 inflammatory cytokine release from both the apical and basolateral surfaces was significantly augmented
302 compared to both the infected epithelial monocultures and the non-infected co-cultures, demonstrating an
303 exacerbation of pro-inflammatory cytokine release in the infected co-cultures (**figure 1b&c**). Compared to the
304 infected epithelial monocultures, infection of the co-culture model resulted in a significant increase in the

305 apical secretion of IFNy, IL1- β , IL-6 and IL10 (1030 \pm 5%, p<0.0001; 169 \pm 6%, p<0.05; 580 \pm 8% p<0.0001 and
306 231 \pm 3%, p<0.001, respectively) (**figure 1b**) and in the basolateral secretion of IFNy, IL1- β , IL-4, IL-6, IL10
307 and TNF α (261 \pm 5%, p<0.05; 572 \pm 6% p<0.0001; 203 \pm 5% p<0.001; 593 \pm 8% p<0.0001; 279 \pm 8% p<0.001 and
308 316 \pm 2%, p<0.001, respectively) (**figure 1c**). Compared to the uninfected neutrophil-epithelial co-cultures, co-
309 culture infection resulted in a significant increase in the apical secretion of IFNy, IL1- β , , IL-6 and IL10
310 (338 \pm 5%, p<0.0001; 161 \pm 6%, p<0.05; 593 \pm 7% p<0.0001 and 136 \pm 3%, p<0.05, respectively) and in the
311 basolateral secretion of IFNy, IL-1 β , IL-4, IL-6 IL10 and TNF α (261 \pm 5% p<0.001; 572 \pm 4% p<0.0001; 227 \pm 5%
312 p<0.0001; 704 \pm 18% p<0.0001; 156 \pm 8%, p<0.001 and 167 \pm 3%, p<0.0001, respectively) (**figure 1b**). The only
313 instance where TNF α was significantly changed in the apical supernatants was in the infected co-cultures
314 when compared to uninfected epithelial cell monocultures with a 329 \pm 13%, p<0.01 increase. This data
315 supports a significant augmentation of the inflammatory response to SARS-CoV-2 infection occurs in the
316 presence of pre-existing airway neutrophilia. Importantly, this secretion profile closely reflects the cytokine
317 biomarkers that have been clinically identified in patients hospitalized with severe COVID-19 disease [43-45],
318 highlighting the importance of the co-culture models in recapitulating features associated with more severe
319 responses to SARS-CoV-2 and demonstrating a role for neutrophils in the inflammatory profile observed in
320 patients with severe COVID-19.

321 **Increased SARS-CoV-2 infection of the airway epithelium is associated with neutrophilia and
322 disruption of epithelial barrier integrity.**

323 To determine whether a proinflammatory niche, such as that observed in the presence of pre-existing
324 neutrophilia, impacts epithelial barrier integrity and viral load of the epithelial cells we evaluated barrier
325 resistance and viral content of the airway epithelium. Trans epithelial electrical resistance (TEER) was
326 recorded at 4 and 24 hours after introduction of neutrophils to the airway epithelium. The presence of
327 neutrophils significantly reduced the TEER and, therefore, epithelial barrier integrity, by 23 \pm 9%, p<0.05 after
328 4 hours. This reduction in TEER was sustained through 24 hours (22 \pm 4%, p<0.05), all data are compared to
329 epithelial monocultures (**figure 2a**). Evaluation of intracellular viral load by qRT-PCR for SARS-CoV-2
330 nucleocapsid RNA in the epithelial cells under the same conditions indicated a concurrent and significant
331 increase in infection after the addition of neutrophils by 3.1 \pm 1.1-fold (p<0.05) (**figure 2b**). In the absence of
332 infection, no SARS-CoV-2 RNA was detected (data not shown). To determine if the change in epithelial barrier

333 function allowed for increased passage of viral particles from the apical to basolateral surface of the airway
334 epithelium, we also evaluated SARS-CoV-2 spike protein expression in the supernatants (**figure 2c-d**). The
335 presence of neutrophils significantly decreased the apical viral load from 69204 ± 9200.1 fg/ml to
336 6655.6 ± 475.61 fg/ml ($p < 0.01$) (**figure 2c**) with a concurrent increase in the basolateral viral load from
337 488.23 ± 129.12 fg/ml to 2307.7 ± 238.94 fg/ml ($p < 0.01$) (**figure 2d**). This data shows that the presence of
338 neutrophils allows for increased migration of virus from the apical to the basolateral surface. To determine
339 whether the physical presence of neutrophils is essential or whether the pro-inflammatory cytokines released
340 from neutrophils in epithelial co-cultures (**figure 2**) and stimulated by SARS-CoV-2 infection, could induce
341 similar changes in epithelial barrier function, we supplemented the culture media with IFNy (10 ng/ml), IL-1 β
342 (10 ng/ml), IL-6 (10 ng/ml) and TNF α (10 ng/ml) (referred to as cytomix). In the presence of cytomix TEER
343 decreased after 4 hours ($18 \pm 7\%$, not significant) with a further and significant decline of $30 \pm 5\%$, $p < 0.05$ after
344 24 hours (**figure 2e**). This decrease in TEER corresponded to an increase in viral infection of the airway
345 epithelium (2.6 ± 0.5 -fold, $p < 0.05$) in the presence of cytomix (**figure 2f**). Reflecting the observations in the
346 presence of neutrophils the apical concentrations of SARS-CoV-2 were decreased from 76703 ± 8708.7 fg/ml
347 to 35261 ± 3598.7 fg/ml ($p < 0.05$) and basolateral concentrations increased from 479.87 ± 129.21 fg/ml to
348 12344 ± 906.62 fg/ml ($p < 0.001$). This data supports the hypothesis that pro-inflammatory cytokines secreted
349 by neutrophils allow for increased transition of virus from the apical to basolateral surfaces of the airway
350 epithelium.

351 **Neutrophils increase SARS-CoV-2 infection of the epithelium including basal stem cells.**

352 To investigate changes in airway pathology associated with SARS-CoV-2 infection we evaluated co-
353 localization of SARS-CoV-2 virus in the presence or absence of neutrophils. Analysis of the airway structure
354 by hematoxylin and eosin (H&E) highlights significant changes in pathology in the presence of neutrophils
355 (**figure 3a-d**). In the absence of neutrophils and infection the airways comprise of a typical airway epithelium
356 with KRT5+ basal cells residing on the basolateral surface and ciliated cells lining the airway lumen (**figure**
357 **3a**). Despite the presence of pro-inflammatory cytokines produced by the neutrophils, epithelial cells appear
358 to tolerate the presence of neutrophils, which can be observed in close proximity to the apical ciliated cells in
359 the culture model (**figure 3b**). In an airway without neutrophils, the epithelial cells are capable of tolerating
360 infection by SARS-CoV-2 after 4 hours of exposure with little evidence of cellular pathology by H&E and only

361 sporadic infection observed in the columnar epithelial cells (**figure 3c and supplemental figure S3**). Most
362 notably, in the presence of neutrophils, significant cellular pathology is observed by H&E, with evidence for
363 thickening of the basal cell layer, indicative of basal cell proliferation (**figure 3d**). Furthermore, SARS-CoV-2
364 infection in epithelium is more widespread across the entire epithelial layer with KRT5+ basal cells also being
365 infected (**figure 3d and supplementary figure S3**). In our model system, neutrophils drive significant cellular
366 pathology and increase basal cell proliferation and infection by SARS-CoV-2. Infection of basal cells at such
367 a short timepoint is likely to have significant implications on their function and subsequently airway
368 regeneration.

369 **Airway epithelial pathologies are associated with neutrophil activity in severe COVID-19.**

370 The data presented from our **in vitro** models suggests that neutrophils play a role in the pathophysiology of
371 early-stage epithelial infection in COVID-19. To further investigate continued neutrophil related pathologies in
372 severe COVID-19 we evaluated epithelial cell related damage and neutrophil activity in post-mortem human
373 tissues from COVID-19 subjects. Formalin-fixed paraffin embedded (FFPE) tissue sections from two post-
374 mortem COVID-19 subjects, kindly provided by the autopsy service at the University of Vermont Medical
375 Center (UVMMC) were assessed for infection-related pathologies through H&E staining. Pathologies were
376 determined by an independent pathologist to be consistent with severe ARDS with mixed inflammatory cell
377 infiltrates, inclusive of neutrophils, and organizing pneumonia (**figure 4a-d**). Tissues from patient Au20-39
378 (detailed in **supplementary table S1**) contained a mild infiltrate of chronic inflammatory cells surrounding the
379 bronchiole and arterial tissues with involvement in the adjacent surrounding alveolar tissue (**figure 4a** and
380 **supplementary figure S4a**). Scattered giant cells were identified in alveolar spaces and within the interstitium
381 (**figure 4b**, indicated by the red arrows and **supplementary figure S4b**). No well-formed granulomas or
382 definite viral inclusions were evident in this patient. Images from the second patient; Au20-48 (**supplementary**
383 **table S1**) also show severe organizing diffuse alveolar damage with evidence of barotrauma (**figure 4c** and
384 **supplementary figure S4d**). Alveolar spaces are lined by hyaline membranes or filled with polyps of
385 organizing pneumonia and chronic inflammation (**supplementary figure S4d**). Alveolar walls are expanded
386 with edema and a mixed inflammatory cell infiltrate including neutrophils (**supplementary figure S4c-d**).
387 Bronchioles demonstrate chronic injury with peribronchiolar metaplasia and early squamous metaplasia
388 (**figure 4d and supplementary figure S4c**). Organizing pulmonary emboli are present in several arteries

389 **(supplementary figure S4c-d)**. There are frequent rounded airspaces lined by inflammatory cells and giant
390 cells, consistent with barotrauma from ventilation injury **(supplementary figure S4d)**. There are also
391 scattered giant cells in the interstitium not associated with the barotrauma **(supplementary figure S4c-d)**.
392 Given the extensive infiltration of inflammatory cells, inclusive of neutrophils, we further evaluated the
393 neutrophil-related epithelial tissue pathology in both patients. An array of airway tissue pathologies was
394 evident in both tissues including 1) basal cell hyperplasia and small airway occlusion **(figure 4e)**, 2) epithelial
395 damage and tissue remodeling of smaller ciliated airways **(figure 4f)**, 3) epithelial shedding of large
396 cartilaginous airways **(figure 4g)**, 4) neutrophil invasion into the airway lumen **(figure 4h)**, and finally, 5)
397 neutrophil invasion in the alveolar space with associated alveolar tissue damage and remodeling
398 **(supplementary figure S4E)**. In each of these examples, neutrophils were detected and frequently
399 demonstrated strong neutrophil elastase (NE) activity **(figure 4e-i)**, and myeloperoxidase (MPO) expression
400 (a common neutrophil marker) is frequently observed around centers of SARS-CoV-2 infection in postmortem
401 COVID-19 tissues **(figure 4f)**. From this data we conclude that neutrophils are a core part of the COVID-19
402 lung pathophysiology and significantly impact airway infection and injury in response to SARS-CoV-2
403 infection.

404 **Phagocytosis of SARS-CoV-2 is the predominant mechanism of viral internalization in neutrophils.**

405 As previously mentioned, airway diseases, such as CF, that are co-morbidities for severe SARS-CoV-2
406 infection and progression to severe COVID-19, are also associated with significant infiltration of the airways
407 with neutrophils **(supplementary figure S5a-b)**. Interestingly, the neutrophils also colocalized with strong
408 ACE2 expression **(supplementary figure S5)**. Despite having significant ACE2 expression our data suggests
409 that internalization of the virus in neutrophils is likely through phagocytosis. The apical concentration of SARS-
410 CoV-2 in the presence of neutrophils was significantly smaller than the apical concentrations of SARS-CoV-
411 2 in the presence of cytomix **(figure 4c&g)** at 6655.65 ± 475.61 fg/ml compared to 35260.93 ± 3598.7 fg/ml,
412 $p < 0.01$. This suggests that viral clearance is taking place by the neutrophils in their functional role as
413 professional phagocytes. In our experiments SARS-CoV-2 viral RNA was detected in the co-cultures by
414 RNAscope confirming infection of the airway epithelium **(figure 5a)**. Interestingly, NE activity was heavily
415 centered around sites of SARS-CoV-2 infection synonymous to that observed in post-mortem patient tissues

416 (supplementary figure S4f), and internalization of SARS-CoV-2 by neutrophils was also confirmed by co-
417 localization of staining for NE and SARS-CoV-2 viral RNA (**figure 5a**) *in vitro*, indicated by the orange arrows.
418 Finally, to determine whether the expression of ACE2 protein in neutrophils has a significant impact in the
419 response of neutrophils to SARS-CoV-2, we evaluated whether neutrophils were being actively infected via
420 a physical interaction of ACE2 and SARS-CoV-2 or functionally phagocytosing the SARS-CoV-2 virus. The
421 decrease in apical spike protein concentrations when neutrophils are present, compared to epithelial cell
422 monocultures, suggests that the neutrophils are clearing the virus at the apical surface through innate pattern
423 recognition phagocytosis. To better understand this, the frequency of SARS-CoV-2 internalization in
424 monocultures of neutrophils was quantified in the presence or absence of cytochalasin D (15 μ M) to inhibit
425 phagocytosis (**figure 5b**). The number of neutrophils positive for SARS-CoV-2 RNA, reflecting viral
426 internalization relative to the total number of neutrophils, was calculated after infection of the cells with SARS-
427 CoV-2 (MOI = 2). Infection, detected by RNA scope, occurred at a rate of 7.9 \pm 1% of neutrophils in culture.
428 This signal was significantly reduced by from 7.9 \pm 1% to 1.3 \pm 0.3% in the presence of cytochalasin D (**Fig.**
429 **5C**). Disruption of the actin cytoskeleton, a core component of phagocytosis, therefore, significantly reduced
430 viral uptake in neutrophils. This suggests the primary mechanism for SARS-CoV-2 internalization in
431 neutrophils is phagocytosis.

432

433

Discussion

434 It is well established that neutrophils are critical in the development of pathological inflammation which can
435 result in both acute and chronic tissue damage. Evaluation of post-mortem COVID-19 tissues indicated
436 significant neutrophil presence and activation in regions of airway epithelial damage and pathology. In
437 addition, we know that many SARS-CoV-2 co-morbidities, including chronic airway disease [30, 46], aging
438 [47-49] and obesity [50-52], are also associated with chronic airway inflammation. In this study we developed
439 a model of pre-existing/chronic airway neutrophilia akin to a model previously developed to investigate other
440 respiratory viruses [27] and applied this to investigate the initial stages of SARS-CoV-2 airway infection. Using
441 this model, we were able to conclude that the pre-existing presence of neutrophils in airway epithelium
442 generates a pro-inflammatory niche, significantly augments initial proinflammatory responses to SARS-CoV-
443 2 infection, increases viral load in basal stem cells and decreases airway epithelial barrier integrity. Our data,
444 therefore, supports a key role for neutrophilic airway inflammation in determining the infectivity and outcome
445 measures of COVID-19.

446 Establishing a primary cell co-culture model of an inflammatory airway overcomes some of the limitations of
447 using immortalized cell lines and more complex *in vivo* models. While *in vivo* models are perhaps considered
448 gold standard in infection models, they have not been observed to closely mimic human lung pathophysiology,
449 particularly with respect to SARS-CoV-2. While infection can be detected, no animal model had closely
450 reflected COVID-19 pathogenesis that leads to severe symptoms and fatal lung disease [5, 53]. Furthermore,
451 studying neutrophilia in animal models is challenging, several depleted or knockout models exist [54], however
452 evaluation of elevated lung neutrophilia typically requires pro-inflammatory stimulation with lipopolysaccharide
453 (LPS) [55], this could complicate interpretation of findings in relation to viral infection. Our models use primary
454 HBECs, some of the first cells exposed to the virus that express endogenous levels of ACE2 and TMPRSS2.
455 This allowed for investigation of the initial stages of SARS-CoV-2 infection and characterization of acute phase
456 inflammatory responses.

457 Neutrophil phenotype and function, including those involved in resolving viral infections, is strongly regulated
458 by signals received from their tissue micro-environment [56], in our study we considered neutrophil responses
459 in the presence of an epithelial micro-environment. Our model mimics components of neutrophilic airway
460 inflammation associated with other chronic lung diseases that have been linked with a predisposition to

461 developing more severe COVID-19 disease. Perhaps our most striking finding is the presence of a differential
462 polarized inflammatory response in response to neutrophils and/or SARS-CoV-2. IL-8, the core
463 chemoattractant for neutrophils [38-40, 57], is secreted only on the basolateral surface of the epithelial
464 monocultures, demonstrates that epithelial cells are capable of recognizing neutrophils within their niche and
465 downregulate this chemokine secretion as a result and that the model recapitulates the directionality required
466 to recruit circulating neutrophils into an infected epithelial environment. Furthermore, despite seeding
467 neutrophils on the apical surface of our model, we observed a predominant pro-inflammatory niche
468 basolaterally, with increases in IL-1 β , IL-4, IL-6 and TNF α . Through paired comparisons to primary airway
469 epithelial cells in monoculture, we were able to demonstrate key differences in the secretion of pro- (IFN γ ,
470 IL1 β , IL-6, IL-8 and TNF α) and anti-inflammatory (IL-4 and IL10) mediators, epithelial barrier integrity and
471 infectivity of epithelial cells (**figures 1-2**), which would have been over-looked in monoculture experiments
472 involving airway infection only. Importantly, the secretion of pro-inflammatory cytokines in our model is
473 consistent with clinical studies that have reported an elevated inflammatory profile associated with severe
474 COVID-19 disease. In patient peripheral blood samples, IL-6 [58-61] IL-10 [59, 60] are consistently higher in
475 COVID-19 patients and correlate with disease severity. Additionally, IL-6 and IL-8 are even higher in ICU than
476 the IMU [62]. Our data also closely mimics responses observed in primate models of the disease [63]. The
477 lack of robust inflammatory response of the epithelium alone may also provide rational for why some people
478 are predisposed to more severe responses than others. In fact, our data evaluating the response of the more
479 proximal, cartilaginous airways may highlight the importance of a robust proximal airway defense mechanism
480 that controls the progression to severe COVID-19 associated with ARDS and distal airway dysfunction.

481 Pro-inflammatory cytokines, including IFN γ , IL1 β , IL-6 and TNF α , have extensively been shown to disrupt
482 barrier integrity and permeability of the epithelium [64, 65]. This breakdown in barrier integrity exists to allow
483 for leukocyte migration to sites of stress and infection. Theoretically, any tight-junction breakdown that allows
484 for more leukocyte migration, would also allow for increased permeability for viral particles to sub-apical and
485 sub-epithelial structures, thus increasing infectivity and cellular viral loads. Our data supports this
486 phenomenon with both neutrophils and cytomix synonymously decreasing barrier integrity (**figure 2**) whilst
487 increasing intracellular viral loads and virus concentrations in sub-apical compartments. This association of

488 epithelial barrier integrity with an increase in intracellular epithelial viral loads, especially in the basal stem
489 cells, suggests that epithelial barrier integrity plays an important functional role in SARS-CoV-2 infection.

490 Finally, we addressed the key question of whether neutrophils, as professional phagocytes [66, 67], are
491 capable of innate recognition of SARS-CoV-2 as an invading pathogen through innate recognition pathways,
492 and/or are capable of infection by SARS-CoV-2 inherently via ACE2 expression. Our data supports a high
493 level of expression of ACE2 at the protein level, but not the RNA level in neutrophils; an observation recently
494 reported by Veras and colleagues [26]. Furthermore, infection is facilitated by TMPRSS2 and we did not see
495 any evidence for expression on neutrophils. By using cytochalasin D to breakdown actin filament organization
496 we significantly reduced internalization, supporting a predominant role for phagocytosis in the internalization
497 of SARS-CoV-2 in neutrophils. Reports are, however, emerging that suggest a significant role for cytoskeletal
498 rearrangement in SARS-CoV-2 entry and, therefore, we cannot entirely rule out infection [68]. The use of
499 blocking antibodies has potential to elucidate the mechanisms of internalization, however, neutrophils express
500 copious amounts of Fc receptors [69] and likely to recognize antigens and opsonize through phagocytosis.
501 Our assay attempted to investigate an innate recognition, i.e. a non-humoral opsonization of the SARS-CoV-
502 2 virus. To determine whether the expression of ACE2 on neutrophils is functionally relevant in SARS-CoV-
503 2 infection further investigation will be essential.

504 In conclusion, we have developed a model to study neutrophil-epithelial interactions which more closely
505 reflects an *in vivo* and more clinically relevant infection of airways than monocultures. Our findings
506 demonstrate that the co-presence of neutrophils generates a polarized pro-inflammatory niche with the
507 conducting airway epithelium that is significantly augmented with SARS-CoV-2 infection. This pro-
508 inflammatory niche breaks down the epithelial barrier integrity allowing for increased epithelial infection
509 including basal stem cells. Overall, this study reveals a key role for pre-existing chronic airway neutrophilia in
510 determining infectivity and outcomes in response to SARS-CoV-2 infection that highlight neutrophilia as a
511 potential target for prevention of severe COVID-19 disease.

512

513 **Acknowledgements**

514 The authors acknowledge the Center for Advanced Research Computing (CARC) at the University of
515 Southern California for providing computing resources that have contributed to the research results reported
516 within this publication. URL: <https://carc.usc.edu>. All Biosafety Level 3 work was performed within The
517 Hastings Foundation and The Wright Foundation Laboratories at USC. SARS-V2 BSL3 resources supported
518 by a grant from the COVID-19 Keck Research Fund. Flow cytometry was performed in the USC Flow
519 Cytometry Facility supported in part by the National Cancer Institute Cancer Center Shared Grant award
520 P30CA014089 and the USC Office of the Provost, Dean's Development Funds, Keck School of Medicine of
521 USC. The content is solely the responsibility of the authors and does not necessarily represent the official
522 views of the National Cancer Institute or the National Institutes of Health. We thank the organ donors and
523 their families for their invaluable donation and the International Institute for the Advancement of Medicine
524 (IIAM), Drs Daniel Weiss and Sharon Mount and the UVMMC autopsy service at the University of Vermont,
525 and Dr. Scott Randell at the University of North Carolina Marsico Lung Institute Tissue Procurement and Cell
526 Culture Core supported in part by NIH DK065988 and grant BOUCHR19R0 from the Cystic Fibrosis
527 Foundation, for their partnership in providing lung tissues for research. Finally, the authors wish to thank the
528 USC COVID-19 Biospecimen Repository for assistance with pathologic analysis

529

530 **Funding**

531 ALR is funded by the Hastings Foundation, Daniel Tyler Health and Education Fund, and the Cystic Fibrosis
532 Foundation (CFFT17XX0 and CFFT21XX0).

533

534 **Author Contributions**

535 Conceptualization, B.A.C and A.L.R.; Methodology; B.A.C and A.L.R.; Formal Analysis, M.P.S.; Investigation,
536 B.A.C, E.J.Q, Z.L., N.D., C.N.S., S.K., W.D.W., J.H., and A.L.R; Writing - Original Draft, B.A.C and A.L.R.,
537 Writing – Review and editing, B.A.C and A.L.R., Funding Acquisition, A.L.R.

538

539 **Declaration of Interests**

540 The authors declare no competing interests

541

542 **Figure Legends**

543 **Figure 1: Polarized inflammatory response of neutrophils in co-culture with human airway epithelium,**
544 **infected with SARS-CoV-2.** a) Schematic of the *in vitro* model of neutrophilic airways denoting neutrophils
545 in co-culture with differentiated airway epithelial cells and infected with live SARS-CoV-2 virus. Inflammatory
546 profiles of apical (b) and basolateral (c) supernatants collected 4 hours post infection in the neutrophilic airway
547 model. Data is expressed as Tukey method box & whiskers plots. Significance is determined by analysis of
548 variance (ANOVA) followed by Tukey's post hoc analysis. *p<0.05, **p<0.01, ***p<0.001, ****p<0.0001 from
549 n=3 experimental repeats from N=3 biological donors.

550 **Figure 2: Neutrophils and pro-inflammatory cytokines break down the epithelial barrier and increase**
551 **viral load in human airway epithelial cells.** a) TEER of human airway epithelial cells at the air-liquid
552 interface in the presence, or absence (control), of neutrophils. b) Intracellular viral load of SARS-CoV-2 RNA
553 isolated from infected human airway epithelial cells with neutrophils present. c) Apical supernatant SARS-
554 CoV-2 spike protein concentration 4 hours post infection with neutrophils present. d) Basolateral supernatant
555 SARS-CoV-2 spike protein concentration 4 hours post infection with neutrophils present. e) TEER of human
556 airway epithelial cells cultured with a "cytomix" of TNF α , IL-1 β , IL-6 and IFN- γ each at 10ng/ml. f) Intracellular
557 viral load of SARS-CoV-2 in airway epithelial cells cultured with cytomix. g) Apical supernatant SARS-CoV-2
558 spike protein concentration 4 hours post infection from epithelial cells cultured with cytomix. h) Basolateral
559 supernatant SARS-CoV-2 spike protein concentration 4 hours post infection from epithelial cells cultured with
560 cytomix. Data are expressed as mean \pm SEM. Statistical significance of TEER data was determined by ANOVA
561 and viral load data was analyzed using an unpaired two-tailed Student's t-test. *p<0.05. Experiments include
562 n=3 experimental repeats of N=3 independent epithelial donors paired with 3 independent neutrophil donors.

563 **Figure 3: A pre-existing pro-inflammatory environment increases SARS-CoV-2 infection of airway**
564 **basal stem cells.** a-d) representative hematoxylin and eosin (H&E) staining and immunofluorescent images
565 of cross section culture models probed for KRT5 (green) Sars-CoV-2 (red) and alpha-tubulin (cyan). a)
566 uninfected monocultured epithelial cells. b) uninfected epithelial cell – neutrophil co-culture. c) SARS-CoV-2
567 infected epithelial cell monoculture. d) SARS-CoV-2 infected epithelial cell – neutrophil co-culture. All IF
568 images have nuclei counterstained with DAPI (blue) and scale bars represent 50 μ m. All images are
569 representative of 3 independent experimental repeats of 3 neutrophil and 3 epithelial random donor pairings.

570 **Figure 4: Neutrophil associated tissue pathology in post-mortem COVID19 human lung airways. a-d)**

571 Representative images of hematoxylin and eosin (H&E) staining of postmortem COVID-19 patient tissues
572 showing patchy organizing pneumonia centered around a major artery and an airway (a); focally expanded
573 interstitium by a mixed cellular infiltrate including scattered giant cells (red arrowheads) (b); diffuse alveolar
574 damage from intense fibroinflammatory process and barotrauma induced rounded airspaces (c) and
575 organizing diffuse alveolar damage with fibrin disposition replaced by organizing pneumonia, inflammatory
576 cells and oedema (d). e-i) Representative IF images of postmortem COVID-19 tissue probed for NE (cyan),
577 KRT5 (green) and ACE2 (red). Images highlight; small airway occlusion resulting from basal cell hyperplasia
578 with surrounding neutrophils present (e); epithelial damage with breaching neutrophils into the luminal space
579 (f); epithelial shedding, inclusive of basal cell layer with neutrophil inclusion of mucosal surface (g); neutrophil
580 breach into airway luminal space with high neutrophil elastase activity (h) and diffuse neutrophil invasion of
581 alveolar spaces (i). All IF images have nuclei counterstained with DAPI (blue) and scale bars represent 100
582 μ m. All images are representative of 3 independent regions per donor at least 2 independent donors.

583 **Figure 5: Cytochalasin D inhibits internalization of SARS-CoV-2 in neutrophils. a)** Representative IF

584 images of ALI cultures probed for neutrophil elastase (NE) (Green) infected with SARS-CoV-2 (red) detected
585 by RNAScope. b) Quantification of SARS-CoV-2 positive neutrophils relative to total number of neutrophils
586 determined by DAPI (blue). Data expressed as mean \pm SEM. **p<0.01 unpaired 2-tailed Student's T-test. N=3
587 independent neutrophil donors, n=3 experimental replicates.

588

589

590

591 **References**

592 1. Wu Z, McGoogan JM. Characteristics of and Important Lessons From the Coronavirus Disease 2019
593 (COVID-19) Outbreak in China: Summary of a Report of 72314 Cases From the Chinese Center for Disease
594 Control and Prevention. *JAMA* 2020; 323(13): 1239-1242.

595 2. Guan WJ, Ni ZY, Hu Y, Liang WH, Ou CQ, He JX, Liu L, Shan H, Lei CL, Hui DSC, Du B, Li LJ, Zeng
596 G, Yuen KY, Chen RC, Tang CL, Wang T, Chen PY, Xiang J, Li SY, Wang JL, Liang ZJ, Peng YX, Wei L, Liu
597 Y, Hu YH, Peng P, Wang JM, Liu JY, Chen Z, Li G, Zheng ZJ, Qiu SQ, Luo J, Ye CJ, Zhu SY, Zhong NS,
598 China Medical Treatment Expert Group for C. Clinical Characteristics of Coronavirus Disease 2019 in China.
599 *N Engl J Med* 2020; 382(18): 1708-1720.

600 3. Pechous RD. With Friends Like These: The Complex Role of Neutrophils in the Progression of Severe
601 Pneumonia. *Front Cell Infect Microbiol* 2017; 7: 160.

602 4. Grommes J, Soehnlein O. Contribution of neutrophils to acute lung injury. *Mol Med* 2011; 17(3-4):
603 293-307.

604 5. Munoz-Fontela C, Dowling WE, Funnell SGP, Gsell PS, Riveros-Balta AX, Albrecht RA, Andersen H,
605 Baric RS, Carroll MW, Cavalieri M, Qin C, Crozier I, Dallmeier K, de Waal L, de Wit E, Delang L, Dohm E,
606 Duprex WP, Falzarano D, Finch CL, Frieman MB, Graham BS, Gralinski LE, Guilfoyle K, Haagmans BL,
607 Hamilton GA, Hartman AL, Herfst S, Kaptein SJF, Klimstra WB, Knezevic I, Krause PR, Kuhn JH, Le Grand
608 R, Lewis MG, Liu WC, Maisonnasse P, McElroy AK, Munster V, Oreshkova N, Rasmussen AL, Rocha-Pereira
609 J, Rockx B, Rodriguez E, Rogers TF, Salguero FJ, Schotsaert M, Stittelaar KJ, Thibaut HJ, Tseng CT,
610 Vergara-Alert J, Beer M, Brasel T, Chan JFW, Garcia-Sastre A, Neyts J, Perlman S, Reed DS, Richt JA, Roy
611 CJ, Segales J, Vasan SS, Henao-Restrepo AM, Barouch DH. Animal models for COVID-19. *Nature* 2020;
612 586(7830): 509-515.

613 6. Zhang B, Zhou X, Zhu C, Song Y, Feng F, Qiu Y, Feng J, Jia Q, Song Q, Zhu B, Wang J. Immune
614 Phenotyping Based on the Neutrophil-to-Lymphocyte Ratio and IgG Level Predicts Disease Severity and
615 Outcome for Patients With COVID-19. *Front Mol Biosci* 2020; 7: 157.

616 7. Song C-Y, Xu J, He J-Q, Lu Y-Q. COVID-19 early warning score: a multi-parameter screening tool to
617 identify highly suspected patients. *medRxiv* 2020; 2020.2003.2005.20031906.

618 8. Aveyard P, Gao M, Lindson N, Hartmann-Boyce J, Watkinson P, Young D, Coupland CAC, Tan PS,
619 Clift AK, Harrison D, Gould DW, Pavord ID, Hippisley-Cox J. Association between pre-existing respiratory
620 disease and its treatment, and severe COVID-19: a population cohort study. *Lancet Respir Med* 2021.

621 9. Galani IE, Andreakos E. Neutrophils in viral infections: Current concepts and caveats. *J Leukoc Biol*
622 2015; 98(4): 557-564.

623 10. Bordon J, Aliberti S, Fernandez-Botran R, Uriarte SM, Rane MJ, Duvvuri P, Peyrani P, Morlacchi LC,
624 Blasi F, Ramirez JA. Understanding the roles of cytokines and neutrophil activity and neutrophil apoptosis in
625 the protective versus deleterious inflammatory response in pneumonia. *Int J Infect Dis* 2013; 17(2): e76-83.

626 11. Borges L, Pithon-Curi TC, Curi R, Hatanaka E. COVID-19 and Neutrophils: The Relationship between
627 Hyperinflammation and Neutrophil Extracellular Traps. *Mediators Inflamm* 2020; 2020: 8829674.

628 12. Huang C, Wang Y, Li X, Ren L, Zhao J, Hu Y, Zhang L, Fan G, Xu J, Gu X, Cheng Z, Yu T, Xia J, Wei
629 Y, Wu W, Xie X, Yin W, Li H, Liu M, Xiao Y, Gao H, Guo L, Xie J, Wang G, Jiang R, Gao Z, Jin Q, Wang J,
630 Cao B. Clinical features of patients infected with 2019 novel coronavirus in Wuhan, China. *Lancet* 2020;
631 395(10223): 497-506.

632 13. Fajgenbaum DC, June CH. Cytokine Storm. *N Engl J Med* 2020; 383(23): 2255-2273.

633 14. Ruan Q, Yang K, Wang W, Jiang L, Song J. Correction to: Clinical predictors of mortality due to
634 COVID-19 based on an analysis of data of 150 patients from Wuhan, China. *Intensive Care Med* 2020; 46(6):
635 1294-1297.

636 15. Chen G, Wu D, Guo W, Cao Y, Huang D, Wang H, Wang T, Zhang X, Chen H, Yu H, Zhang X, Zhang
637 M, Wu S, Song J, Chen T, Han M, Li S, Luo X, Zhao J, Ning Q. Clinical and immunological features of severe
638 and moderate coronavirus disease 2019. *The Journal of clinical investigation* 2020; 130(5): 2620-2629.

639 16. Hemmat N, Derakhshani A, Bannazadeh Baghi H, Silvestris N, Baradaran B, De Summa S.
640 Neutrophils, Crucial, or Harmful Immune Cells Involved in Coronavirus Infection: A Bioinformatics Study.
641 *Frontiers in genetics* 2020; 11: 641.

642 17. Shi H, Zuo Y, Yalavarthi S, Gockman K, Zuo M, Madison JA, Blair CN, Woodard W, Lezak SP, Lugogo
643 NL, Woods RJ, Lood C, Knight JS, Kanthi Y. Neutrophil calprotectin identifies severe pulmonary disease in
644 COVID-19. *medRxiv* 2020.

645 18. Veras FP, Pontelli M, Silva C, Toller-Kawahisa J, de Lima M, Nascimento D, Schneider A, Caetite D,
646 Rosales R, Colon D, Martins R, Castro I, Almeida G, Lopes MI, Benatti M, Bonjorno L, Giannini M, Luppino-
647 Assad R, Almeida S, Vilar F, Santana R, Bollela V, Martins M, Miranda C, Borges M, Pazin-Filho A, Cunha
648 L, Zamboni D, Dal-Pizzol F, Leiria L, Siyuan L, Batah S, Fabro A, Mauad T, Dolhnikoff M, Duarte-Neto A,
649 Saldiva P, Cunha T, Alves-Filho JC, Arruda E, Louzada-Junior P, Oliveira R, Cunha F. SARS-CoV-2 triggered
650 neutrophil extracellular traps (NETs) mediate COVID-19 pathology. *medRxiv* 2020:
651 2020.2006.2008.20125823.

652 19. Radermecker C, Sabatel C, Vanwinge C, Ruscitti C, Marechal P, Perin F, Schyns J, Rocks N,
653 Toussaint M, Cataldo D, Johnston SL, Bureau F, Marichal T. Locally instructed CXCR4(hi) neutrophils trigger
654 environment-driven allergic asthma through the release of neutrophil extracellular traps. *Nat Immunol* 2019:
655 20(11): 1444-1455.

656 20. Li G, He X, Zhang L, Ran Q, Wang J, Xiong A, Wu D, Chen F, Sun J, Chang C. Assessing ACE2
657 expression patterns in lung tissues in the pathogenesis of COVID-19. *J Autoimmun* 2020: 112: 102463.

658 21. Tomar B, Anders HJ, Desai J, Mulay SR. Neutrophils and Neutrophil Extracellular Traps Drive
659 Necroinflammation in COVID-19. *Cells* 2020: 9(6).

660 22. Qin C, Zhou L, Hu Z, Zhang S, Yang S, Tao Y, Xie C, Ma K, Shang K, Wang W, Tian DS. Dysregulation
661 of Immune Response in Patients With Coronavirus 2019 (COVID-19) in Wuhan, China. *Clinical infectious
662 diseases : an official publication of the Infectious Diseases Society of America* 2020: 71(15): 762-768.

663 23. Veras FP, Pontelli MC, Silva CM, Toller-Kawahisa JE, de Lima M, Nascimento DC, Schneider AH,
664 Caetite D, Tavares LA, Paiva IM, Rosales R, Colon D, Martins R, Castro IA, Almeida GM, Lopes MIF, Benatti
665 MN, Bonjorno LP, Giannini MC, Luppino-Assad R, Almeida SL, Vilar F, Santana R, Bollela VR, Auxiliadora-
666 Martins M, Borges M, Miranda CH, Pazin-Filho A, da Silva LLP, Cunha LD, Zamboni DS, Dal-Pizzol F, Leiria
667 LO, Siyuan L, Batah S, Fabro A, Mauad T, Dolhnikoff M, Duarte-Neto A, Saldiva P, Cunha TM, Alves-Filho
668 JC, Arruda E, Louzada-Junior P, Oliveira RD, Cunha FQ. SARS-CoV-2-triggered neutrophil extracellular traps
669 mediate COVID-19 pathology. *J Exp Med* 2020: 217(12).

670 24. Arcanjo A, Logullo J, Menezes CCB, de Souza Carvalho Giangiarulo TC, Dos Reis MC, de Castro
671 GMM, da Silva Fontes Y, Todeschini AR, Freire-de-Lima L, Decote-Ricardo D, Ferreira-Pereira A, Freire-de-
672 Lima CG, Barroso SPC, Takiya C, Conceicao-Silva F, Savino W, Morrot A. The emerging role of neutrophil

673 extracellular traps in severe acute respiratory syndrome coronavirus 2 (COVID-19). *Sci Rep* 2020: 10(1):
674 19630.

675 25. Janiuk K, Jablonska E, Garley M. Significance of NETs Formation in COVID-19. *Cells* 2021: 10(1).

676 26. Veras FP, Pontelli MC, Silva CM, Toller-Kawahisa JE, de Lima M, Nascimento DC, Schneider AH,
677 Caetité D, Tavares LA, Paiva IM, Rosales R, Colón D, Martins R, Castro IA, Almeida GM, Lopes MIF, Benatti
678 MN, Bonjorno LP, Giannini MC, Luppino-Assad R, Almeida SL, Vilar F, Santana R, Bollela VR, Auxiliadora-
679 Martins M, Borges M, Miranda CH, Pazin-Filho A, da Silva LLP, Cunha LD, Zamboni DS, Dal-Pizzol F, Leiria
680 LO, Siyuan L, Batah S, Fabro A, Mauad T, Dolhnikoff M, Duarte-Neto A, Saldiva P, Cunha TM, Alves-Filho
681 JC, Arruda E, Louzada-Junior P, Oliveira RD, Cunha FQ. SARS-CoV-2-triggered neutrophil extracellular
682 traps mediate COVID-19 pathology. *Journal of Experimental Medicine* 2020: 217(12).

683 27. Deng Y, Herbert JA, Robinson E, Ren L, Smyth RL, Smith CM. Neutrophil-Airway Epithelial
684 Interactions Result in Increased Epithelial Damage and Viral Clearance during Respiratory Syncytial Virus
685 Infection. *J Virol* 2020: 94(13).

686 28. Randell SH, Walstad L, Schwab UE, Grubb BR, Yankaskas JR. Isolation and culture of airway
687 epithelial cells from chronically infected human lungs. *In Vitro Cell Dev Biol Anim* 2001: 37(8): 480-489.

688 29. Pfaffl MW. A new mathematical model for relative quantification in real-time RT-PCR. *Nucleic Acids
689 Res* 2001: 29(9): e45.

690 30. Jasper AE, McIver WJ, Sapey E, Walton GM. Understanding the role of neutrophils in chronic
691 inflammatory airway disease. *F1000Res* 2019: 8.

692 31. Thomson GA, Fisher BM, Gemmell CG, MacCuish AC, Gallacher SJ. Attenuated neutrophil
693 respiratory burst following acute hypoglycaemia in diabetic patients and normal subjects. *Acta Diabetol* 1997:
694 34(4): 253-256.

695 32. Taylor S, Dirir O, Zamanian RT, Rabinovitch M, Thompson AAR. The Role of Neutrophils and
696 Neutrophil Elastase in Pulmonary Arterial Hypertension. *Front Med (Lausanne)* 2018: 5: 217.

697 33. Florentin J, Zhao J, Tai YY, Vasamsetti SB, O'Neil SP, Kumar R, Arunkumar A, Watson A, Sembrat
698 J, Bullock GC, Sanders L, Kassa B, Rojas M, Graham BB, Chan SY, Dutta P. Interleukin-6 mediates
699 neutrophil mobilization from bone marrow in pulmonary hypertension. *Cell Mol Immunol* 2021: 18(2): 374-
700 384.

701 34. Zhu N, Wang W, Liu Z, Liang C, Wang W, Ye F, Huang B, Zhao L, Wang H, Zhou W, Deng Y, Mao L,
702 Su C, Qiang G, Jiang T, Zhao J, Wu G, Song J, Tan W. Morphogenesis and cytopathic effect of SARS-CoV-
703 2 infection in human airway epithelial cells. *Nat Commun* 2020; 11(1): 3910.

704 35. Jia HP, Look DC, Shi L, Hickey M, Pewe L, Netland J, Farzan M, Wohlford-Lenane C, Perlman S,
705 McCray PB, Jr. ACE2 receptor expression and severe acute respiratory syndrome coronavirus infection
706 depend on differentiation of human airway epithelia. *J Virol* 2005; 79(23): 14614-14621.

707 36. Jia HP, Look DC, Tan P, Shi L, Hickey M, Gakhar L, Chappell MC, Wohlford-Lenane C, McCray PB,
708 Jr. Ectodomain shedding of angiotensin converting enzyme 2 in human airway epithelia. *Am J Physiol Lung
709 Cell Mol Physiol* 2009; 297(1): L84-96.

710 37. Zhang H, Rostami MR, Leopold PL, Mezey JG, O'Beirne SL, Strulovici-Barel Y, Crystal RG.
711 Expression of the SARS-CoV-2 ACE2 Receptor in the Human Airway Epithelium. *Am J Respir Crit Care Med
712* 2020; 202(2): 219-229.

713 38. Baggolini M, Walz A, Kunkel SL. Neutrophil-activating peptide-1/interleukin 8, a novel cytokine that
714 activates neutrophils. *The Journal of clinical investigation* 1989; 84(4): 1045-1049.

715 39. Yoshimura T, Matsushima K, Tanaka S, Robinson EA, Appella E, Oppenheim JJ, Leonard EJ.
716 Purification of a human monocyte-derived neutrophil chemotactic factor that has peptide sequence similarity
717 to other host defense cytokines. *Proc Natl Acad Sci U S A* 1987; 84(24): 9233-9237.

718 40. Parsons PE, Fowler AA, Hyers TM, Henson PM. Chemotactic activity in bronchoalveolar lavage fluid
719 from patients with adult respiratory distress syndrome. *Am Rev Respir Dis* 1985; 132(3): 490-493.

720 41. Azevedo MLV, Zanchettin AC, Vaz de Paula CB, Motta Junior JDS, Malaquias MAS, Raboni SM, Neto
721 PC, Zeni RC, Prokopenko A, Borges NH, Godoy TM, Benevides APK, de Souza DG, Baena CP, Machado-
722 Souza C, de Noronha L. Lung Neutrophilic Recruitment and IL-8/IL-17A Tissue Expression in COVID-19.
723 *Front Immunol* 2021; 12: 656350.

724 42. Pease JE, Sabroe I. The role of interleukin-8 and its receptors in inflammatory lung disease:
725 implications for therapy. *Am J Respir Med* 2002; 1(1): 19-25.

726 43. Del Valle DM, Kim-Schulze S, Huang HH, Beckmann ND, Nirenberg S, Wang B, Lavin Y, Swartz TH,
727 Madduri D, Stock A, Marron TU, Xie H, Patel M, Tuballes K, Van Oekelen O, Rahman A, Kovatch P, Aberg
728 JA, Schadt E, Jagannath S, Mazumdar M, Charney AW, Firpo-Betancourt A, Mendum DR, Jhang J, Reich D,

729 Sigel K, Cordon-Cardo C, Feldmann M, Parekh S, Merad M, Gnjatic S. An inflammatory cytokine signature
730 predicts COVID-19 severity and survival. *Nat Med* 2020; 26(10): 1636-1643.

731 44. Han H, Ma Q, Li C, Liu R, Zhao L, Wang W, Zhang P, Liu X, Gao G, Liu F, Jiang Y, Cheng X, Zhu C,
732 Xia Y. Profiling serum cytokines in COVID-19 patients reveals IL-6 and IL-10 are disease severity predictors.
733 *Emerg Microbes Infect* 2020; 9(1): 1123-1130.

734 45. Liu QQ, Cheng A, Wang Y, Li H, Hu L, Zhao X, Wang T, He F. Cytokines and their relationship with
735 the severity and prognosis of coronavirus disease 2019 (COVID-19): a retrospective cohort study. *BMJ Open*
736 2020; 10(11): e041471.

737 46. Gernez Y, Tirouvanziam R, Chanez P. Neutrophils in chronic inflammatory airway diseases: can we
738 target them and how? *Eur Respir J* 2010; 35(3): 467-469.

739 47. Kulkarni U, Zemans RL, Smith CA, Wood SC, Deng JC, Goldstein DR. Excessive neutrophil levels in
740 the lung underlie the age-associated increase in influenza mortality. *Mucosal Immunol* 2019; 12(2): 545-554.

741 48. Chen MM, Palmer JL, Plackett TP, Deburghgraeve CR, Kovacs EJ. Age-related differences in the
742 neutrophil response to pulmonary pseudomonas infection. *Exp Gerontol* 2014; 54: 42-46.

743 49. Sapey E, Patel JM, Greenwood HL, Walton GM, Hazeldine J, Sadhra C, Parekh D, Dancer RCA,
744 Nightingale P, Lord JM, Thickett DR. Pulmonary Infections in the Elderly Lead to Impaired Neutrophil
745 Targeting, Which Is Improved by Simvastatin. *Am J Respir Crit Care Med* 2017; 196(10): 1325-1336.

746 50. Kordonowy LL, Burg E, Lenox CC, Gauthier LM, Petty JM, Antkowiak M, Palvinskaya T, Ubags N,
747 Rincon M, Dixon AE, Vernooy JH, Fessler MB, Poynter ME, Suratt BT. Obesity is associated with neutrophil
748 dysfunction and attenuation of murine acute lung injury. *Am J Respir Cell Mol Biol* 2012; 47(1): 120-127.

749 51. Maia LA, Cruz FF, de Oliveira MV, Samary CS, Fernandes MVS, Trivelin SAA, Rocha NN, Gama de
750 Abreu M, Pelosi P, Silva PL, Rocco PRM. Effects of Obesity on Pulmonary Inflammation and Remodeling in
751 Experimental Moderate Acute Lung Injury. *Front Immunol* 2019; 10: 1215.

752 52. Manicone AM, Gong K, Johnston LK, Giannandrea M. Diet-induced obesity alters myeloid cell
753 populations in naive and injured lung. *Respir Res* 2016; 17: 24.

754 53. Kumar S, Yadav PK, Srinivasan R, Perumal N. Selection of animal models for COVID-19 research.
755 *Virusdisease* 2020; 1-6.

756 54. Stackowicz J, Jonsson F, Reber LL. Mouse Models and Tools for the in vivo Study of Neutrophils.

757 *Front Immunol* 2019; 10: 3130.

758 55. Corteling R, Wyss D, Trifilieff A. In vivo models of lung neutrophil activation. Comparison of mice and

759 hamsters. *BMC Pharmacol* 2002; 2: 1.

760 56. Parkos CA. Neutrophil-Epithelial Interactions: A Double-Edged Sword. *Am J Pathol* 2016; 186(6):

761 1404-1416.

762 57. Kunkel SL, Standiford T, Kasahara K, Strieter RM. Interleukin-8 (IL-8): the major neutrophil

763 chemotactic factor in the lung. *Exp Lung Res* 1991; 17(1): 17-23.

764 58. Yang PH, Ding YB, Xu Z, Pu R, Li P, Yan J, Liu JL, Meng FP, Huang L, Shi L, Jiang TJ, Qin EQ, Zhao

765 M, Zhang DW, Zhao P, Yu LX, Wang ZH, Hong ZX, Xiao ZH, Xi Q, Zhao DX, Yu P, Zhu CZ, Chen Z, Zhang

766 SG, Ji JS, Wang FS, Cao GW. Increased circulating level of interleukin-6 and CD8(+) T cell exhaustion are

767 associated with progression of COVID-19. *Infect Dis Poverty* 2020; 9(1): 161.

768 59. Liu J, Li S, Liu J, Liang B, Wang X, Wang H, Li W, Tong Q, Yi J, Zhao L, Xiong L, Guo C, Tian J, Luo

769 J, Yao J, Pang R, Shen H, Peng C, Liu T, Zhang Q, Wu J, Xu L, Lu S, Wang B, Weng Z, Han C, Zhu H, Zhou

770 R, Zhou H, Chen X, Ye P, Zhu B, Wang L, Zhou W, He S, He Y, Jie S, Wei P, Zhang J, Lu Y, Wang W, Zhang

771 L, Li L, Zhou F, Wang J, Dittmer U, Lu M, Hu Y, Yang D, Zheng X. Longitudinal characteristics of lymphocyte

772 responses and cytokine profiles in the peripheral blood of SARS-CoV-2 infected patients. *EBioMedicine* 2020;

773 55: 102763.

774 60. Godkin A, Humphreys IR. Elevated interleukin-6, interleukin-10 and neutrophil : lymphocyte ratio as

775 identifiers of severe coronavirus disease 2019. *Immunology* 2020; 160(3): 221-222.

776 61. Huang H, Zhang M, Chen C, Zhang H, Wei Y, Tian J, Shang J, Deng Y, Du A, Dai H. Clinical

777 characteristics of COVID-19 in patients with preexisting ILD: A retrospective study in a single center in Wuhan,

778 China. *J Med Virol* 2020; 92(11): 2742-2750.

779 62. Pandolfi L, Fossali T, Frangipane V, Bozzini S, Morosini M, D'Amato M, Lettieri S, Urtis M, Di Toro A,

780 Saracino L, Percivalle E, Tomaselli S, Cavagna L, Cova E, Mojoli F, Bergomi P, Ottolina D, Lilleri D, Corsico

781 AG, Arbustini E, Colombo R, Meloni F. Broncho-alveolar inflammation in COVID-19 patients: a correlation

782 with clinical outcome. *BMC Pulm Med* 2020; 20(1): 301.

783 63. Fahlberg MD, Blair RV, Doyle-Meyers LA, Midkiff CC, Zenere G, Russell-Lodrigue KE, Monjure CJ,
784 Haupt EH, Penney TP, Lehmicke G, Threeton BM, Golden N, Datta PK, Roy CJ, Bohm RP, Maness NJ,
785 Fischer T, Rappaport J, Vaccari M. Cellular events of acute, resolving or progressive COVID-19 in SARS-
786 CoV-2 infected non-human primates. *Nat Commun* 2020; 11(1): 6078.

787 64. Capaldo CT, Nusrat A. Cytokine regulation of tight junctions. *Biochim Biophys Acta* 2009; 1788(4):
788 864-871.

789 65. Al-Sadi R, Boivin M, Ma T. Mechanism of cytokine modulation of epithelial tight junction barrier. *Front
790 Biosci (Landmark Ed)* 2009; 14: 2765-2778.

791 66. Silva MT, Correia-Neves M. Neutrophils and macrophages: the main partners of phagocyte cell
792 systems. *Front Immunol* 2012; 3: 174.

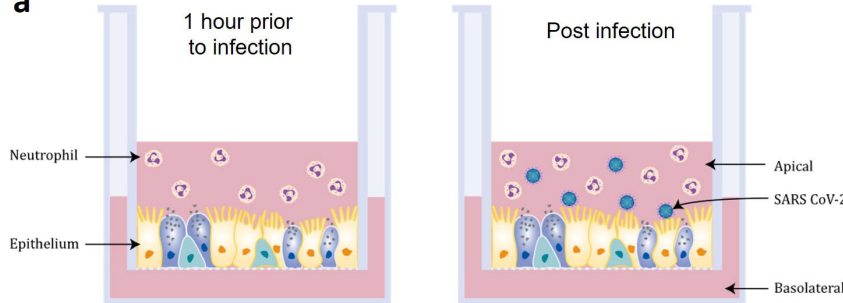
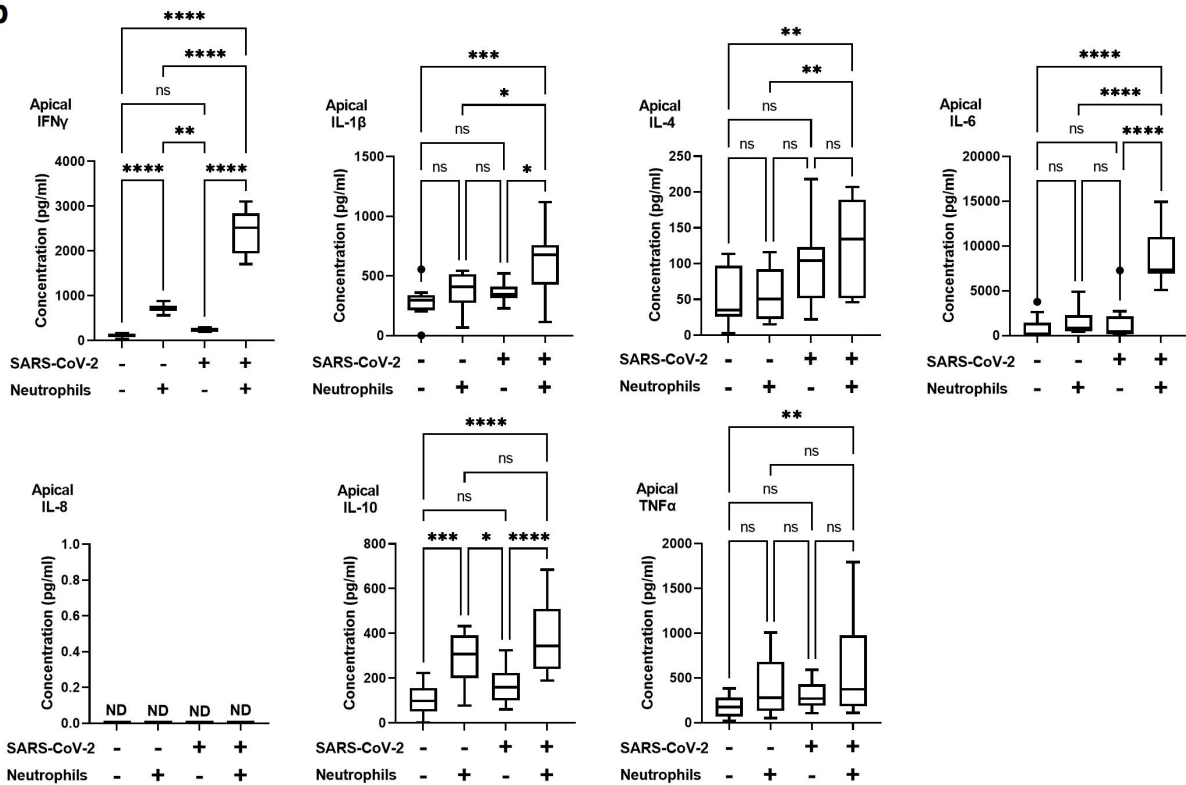
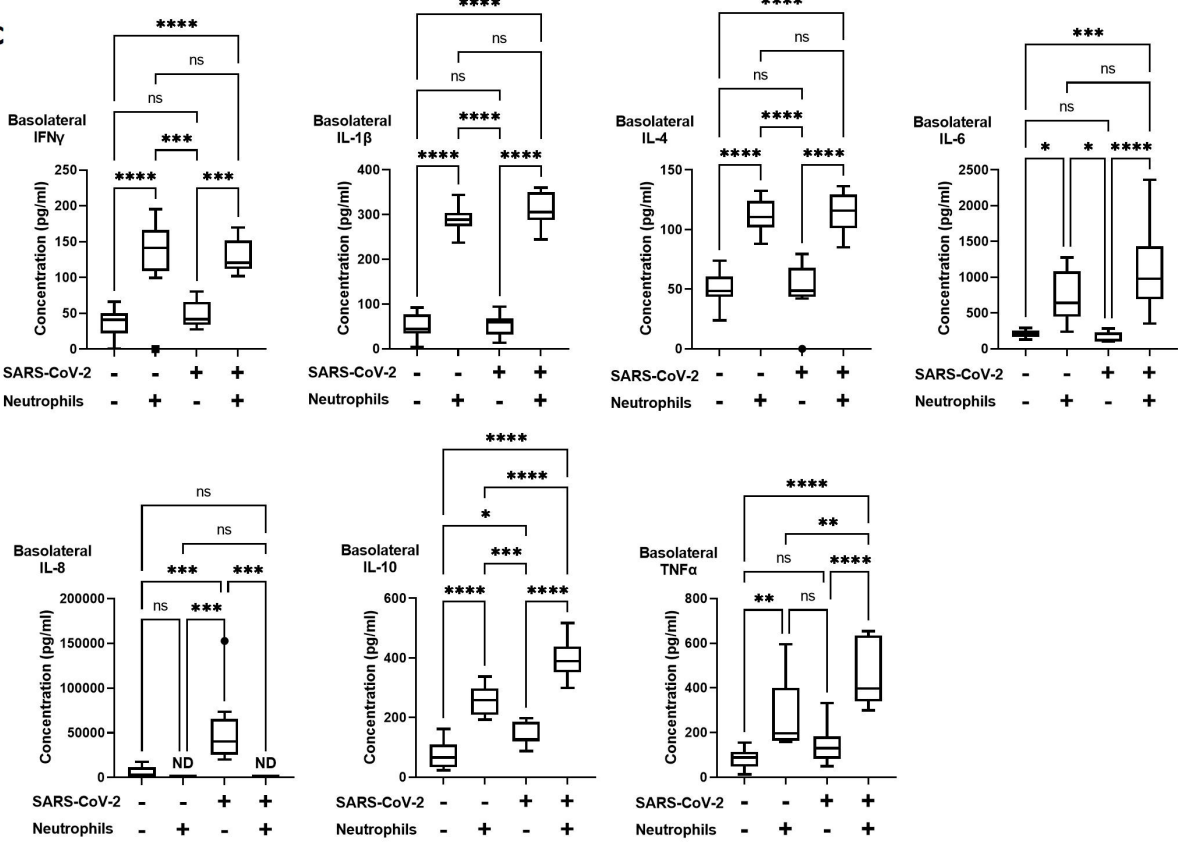
793 67. Uribe-Querol E, Rosales C. Phagocytosis: Our Current Understanding of a Universal Biological
794 Process. *Front Immunol* 2020; 11: 1066.

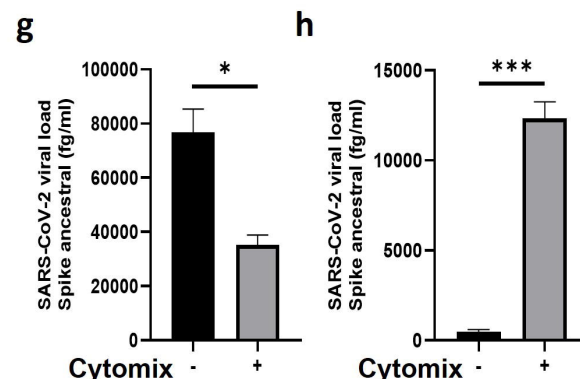
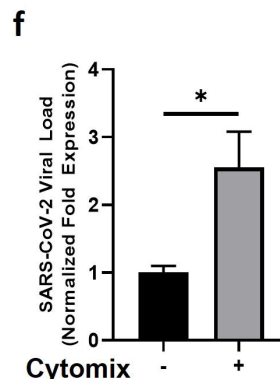
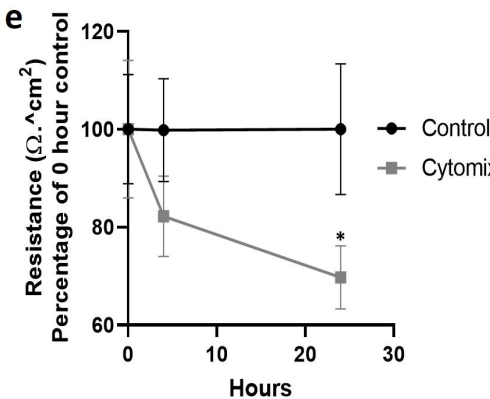
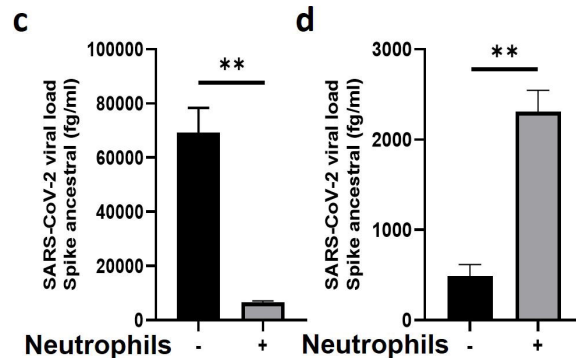
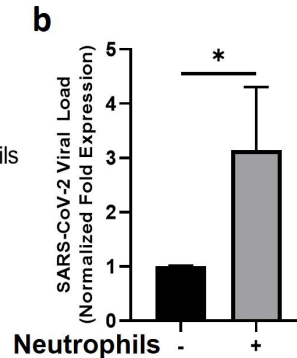
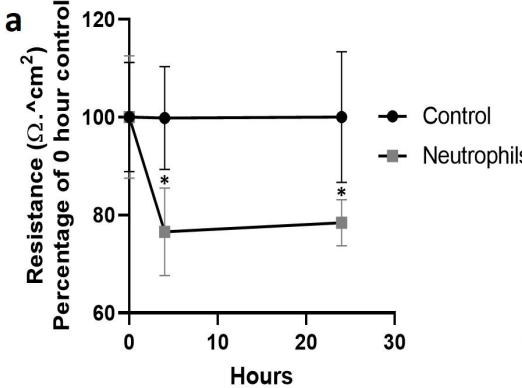
795 68. Wen Z, Zhang Y, Lin Z, Shi K, Jiu Y. Cytoskeleton-a crucial key in host cell for coronavirus infection.
796 *J Mol Cell Biol* 2020; 12(12): 968-979.

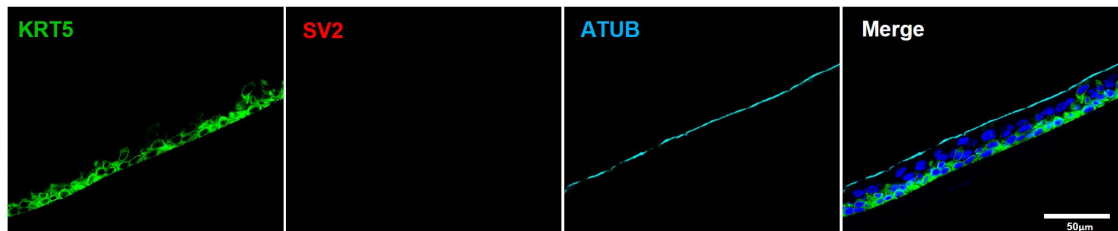
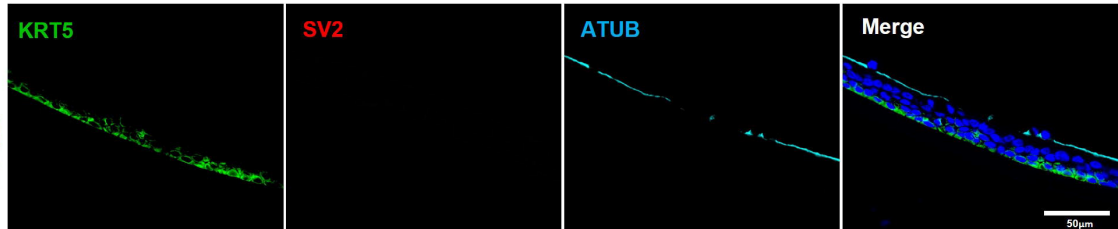
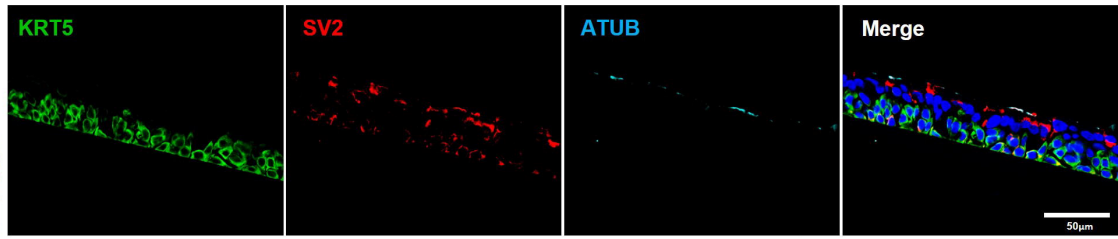
797 69. Wang Y, Jonsson F. Expression, Role, and Regulation of Neutrophil Fcgamma Receptors. *Front
798 Immunol* 2019; 10: 1958.

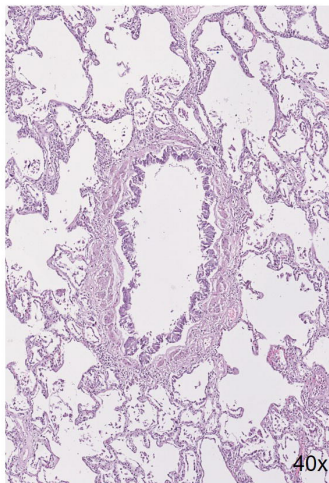
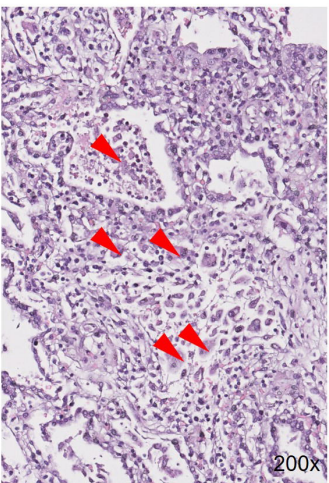
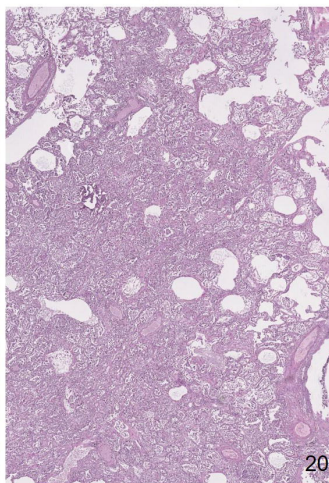
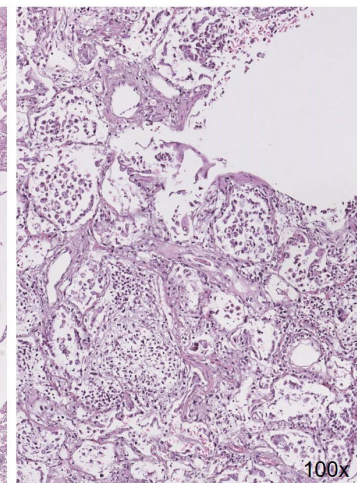
799

800

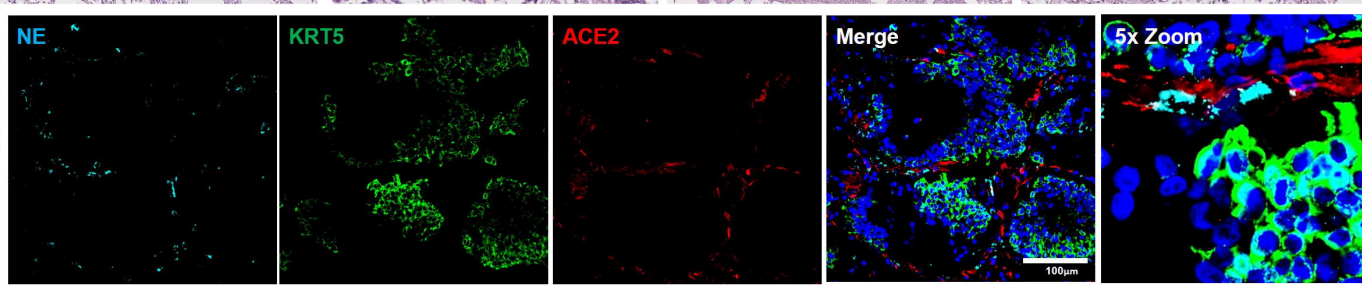
a**b****c**



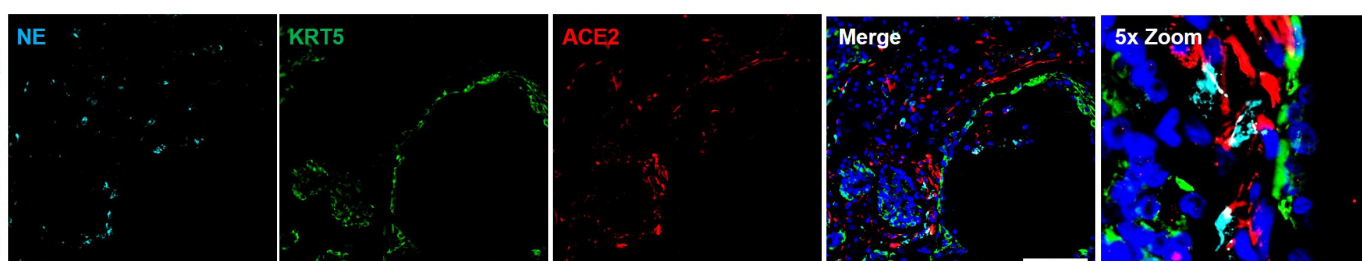
a**b****c****d**

a Patient Au20-39**b** Patient Au20-39**c** Patient Au20-43**d** Patient Au20-43**e**

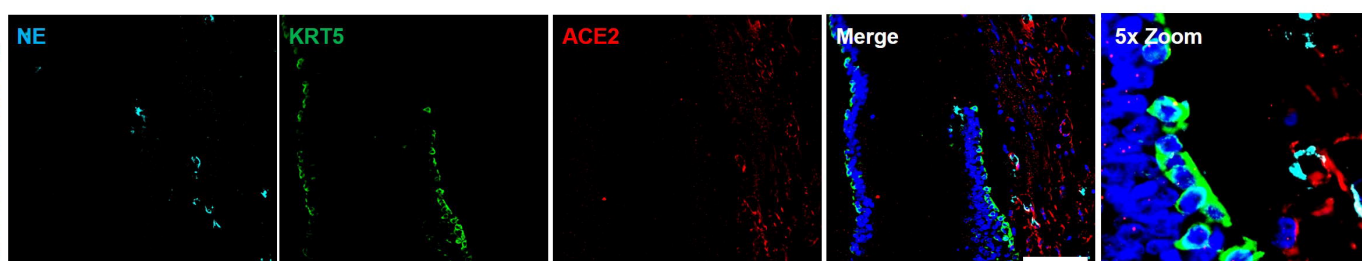
Basal Cell Hyperplasia

**f**

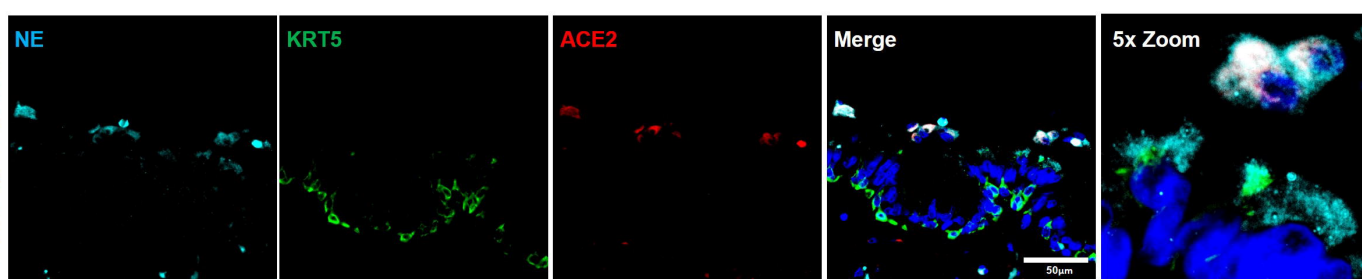
Epithelial damage

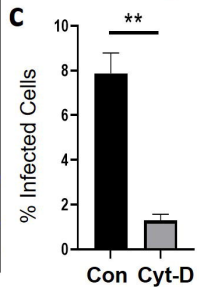
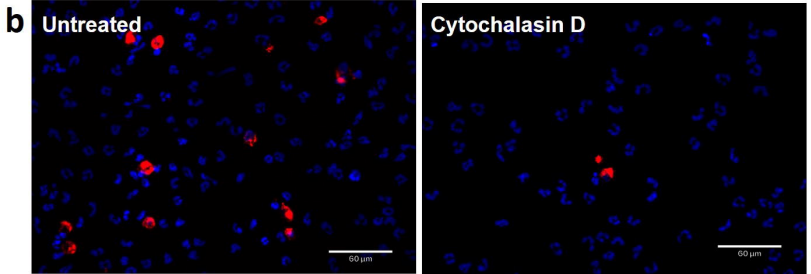
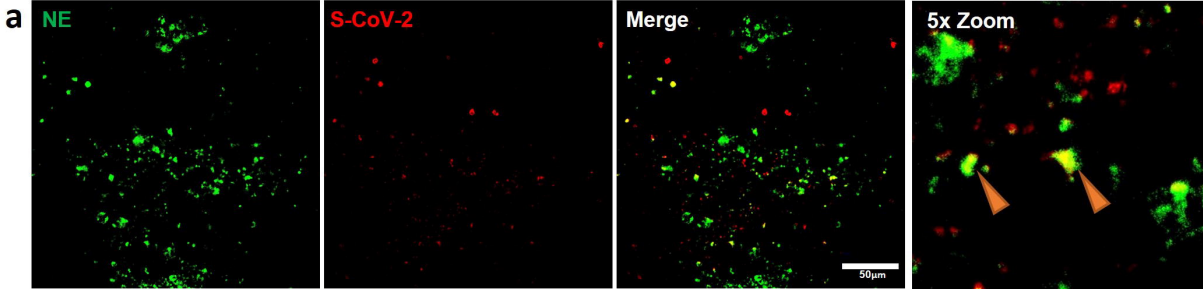
**g**

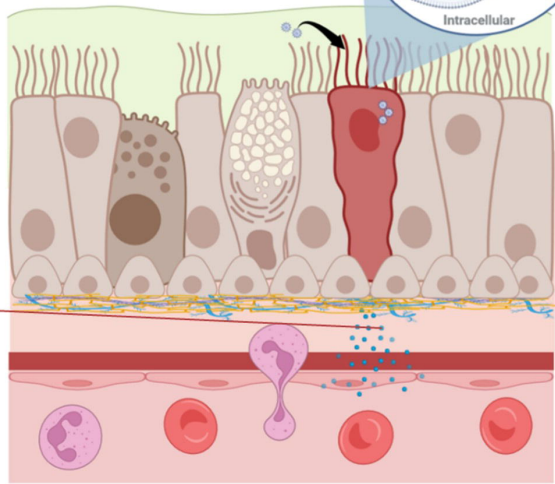
Epithelial Shedding

**h**

Neutrophil breach

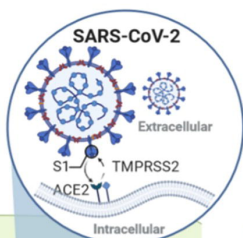
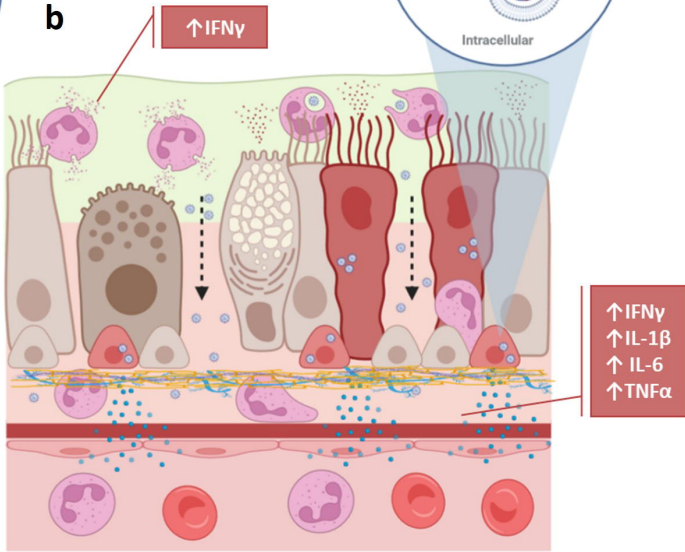




a

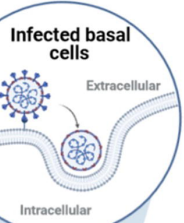
Healthy homeostatic airway

- Tolerated SARS-CoV-2 infection
- Controlled polarized inflammatory response

**b**

Pre-existing neutrophilic airway

- Elevated inflammation impairing epithelial barrier integrity
- Increased infection in sub-apical compartments



\uparrow IFN γ
 \uparrow IL-1 β
 \uparrow IL-6
 \uparrow TNF α